Czech Technical University in Prague

CFD SIMULATION OF SEDIMENTATION OF SMALL PARTICLES

Master Thesis

Özgür Tarık KAPLAN

Faculty of Mechanical Engineering
Department of Process Engineering
Supervisor: Assoc. Prof. Ing. Karel Petera, Ph.D.

Prague, August 2021

MASTER'S THESIS ASSIGNMENT

I. Personal and study details

Student's name: **Kaplan Özgür Tarik** Personal ID number: **490994**

Faculty / Institute: **Faculty of Mechanical Engineering**

Department / Institute: **Department of Process Engineering**

Study program: **Mechanical Engineering**

Branch of study: **Process Engineering**

II. Master's thesis details

Master's thesis title in English:

CFD simulation of sedimentation of small particles

Master's thesis title in Czech:

CFD simulace usazování malých částic

Guidelines:

- Make a literature research concerning possible approaches for modeling of sedimentation of small solid particles in liquid.
- Create models in ANSYS Fluent software and describe settings of the solver for two basic approaches, Euler-Euler and DDPM.
- Perform simulations of sedimentation of particles in a water column and make comparison and analysis of the results.
- Summarize the results and propose possible improvements in future work.

Bibliography / sources:

According to the recommendation of Thesis supervisor.

Name and workplace of master's thesis supervisor:

doc. Ing. Karel Petera, Ph.D., Department of Process Engineering, FME

Name and workplace of second master's thesis supervisor or consultant:

Date of master's thesis assignment: **21.04.2021** Deadline for master's thesis submission: **06.08.2021**

Assignment valid until: **19.09.2021**

doc. Ing. Karel Petera, Ph.D.	prof. Ing. Tomáš Jirout, Ph.D.	prof. Ing. Michael Valášek, DrSc.
Supervisor's signature	Head of department's signature	Dean's signature

III. Assignment receipt

The student acknowledges that the master's thesis is an individual work. The student must produce his thesis without the assistance of others, with the exception of provided consultations. Within the master's thesis, the author must state the names of consultants and include a list of references.

.	
Date of assignment receipt	Student's signature

I confirm that the diploma work was disposed by myself and independently, under leading of my thesis supervisor. I stated all sources of the documents and literature.

In Prague, ...

.....

Özgür Tarık KAPLAN

Acknowledgements

I'd like to express my sincere gratitude to my supervisor, Assoc. Prof. Ing. Karel Petera, Ph.D. for his guidance and feedback throughout this thesis. His insightful feedback helped me to sharpen my thinking to complete this work.

I'd also like to express my love and affection towards my family, who supported me and my decisions under any circumstances. I'm also grateful to my girlfriend Qinyu Liu, who encourage me when I needed it most, I couldn't have completed this without their support.

Annotation sheet

Name: Özgür Tarık

Surname: Kaplan

Title Czech: CFD simulace usazování malých částic

Title English: CFD simulation of sedimentation of small particles

Scope of work: number of pages: 69

number of figures: 71

number of tables: 8

number of appendices: 0

Academic year: 2020/2021

Language: English

Department: Mechanical Engineering

Specialization Process Engineering

Supervisor: Assoc. Prof. Ing. Karel Petera, Ph.D.

Reviewer:

Submitter: Czech Technical University in Prague, Faculty of Mechanical Engineering, Department of Process Engineering

Annotation - Czech: Tato práce byla zaměřena na nalezení optimálních časových kroků a nastavení CFD simulace sedimentace malých částic v softwaru ANSYS Fluent s využitím modelů Euler-Granular a DDPM-KTGF. Byla provedena analýza reálné lamelové geometrie a určena efektivita s ohledem na různé parametry, jako úhel sklonu a rychlost proudění. Byla stanovena kritická rychlost odpovídající 99% efektivitě.

Annotation – English: This work focused on finding optimal time steps and model setup for the CFD simulation of sedimentation of small particles on ANSYS Fluent software by using Euler-Granular and DDPM-KTGF models. Analysis of real lamella geometry was performed to observe

effectiveness for different factors, like inclination angles and velocity magnitudes. The critical velocity for 99% effectiveness was determined.

Keywords: CFD, Sedimentation, Grid Convergency Index, Lamella clarifier, Inclination angle, Velocity magnitude, Effectiveness

Utilization: For Department of Process Engineering, Czech Technical University in Prague

Abstract

The present work focused to find optimal time steps and model setup for the CFD simulation of sedimentation of small particles and performed analysis on real lamella geometry to observe effectiveness for different factors, like inclination angles and velocity magnitudes.

The work of this thesis has been conducted by CFD analysis in ANSYS Fluent software. The preliminary analyses ran with the Euler-Granular and DDPM-KTGF models. The obtained data have been compared for various time steps and their error rates (%) to reduce the analysis time by calculating the grid convergence index. The similarity analysis has been done and compared with real-sized particles experiment data so that bigger-sized particles could be used to decrease computational requirements. The effect of different inclination angles and velocity magnitudes for laminar and turbulent regimes on the lamella geometry was observed for bigger-sized particles. The sedimentation effectiveness of the lamella geometry according to ratio of particles leaving the outlet was evaluated. The critical velocities have been calculated for specific effectiveness 99 (%) .

The study can be improved by widening the number of analyses to find the optimum inclination angle and velocity for the desired design of a lamella clarifier. The lamella clarifier process can be faster by using a two-step lamella clarifier. The first clarifier tank can have a higher velocity magnitude to reduce the number of particles faster during the first step and the second clarifier tank can have the optimal velocity to obtain higher effectiveness for the device.

Keywords: CFD, Sedimentation, Grid Convergency Index, Lamella clarifier, Inclination angle, Velocity magnitude, Effectiveness

List of Tables

List of Figures

List of Symbols

Latin Letters

a : Model parameter

C_{Dt} : Drag coefficient

c_μ : Specific Heat capacity of fluid $[J/kg.k]$

d_p : Particle diameter [mm]

D : Diameter

e_a : Relative error

F : Drag Force $[N]$

F_v : Buoyant force $[N]$

F_s : Inertial force due to acceleration $[N]$

F_g : Gravitational forces on the particle [N]

F_d : Drag forces on the particle [N]

F_b : Buoyant forces on the particle [N]

G : Gravitation force $[N]$

g : Gravitational force $[m/s^2]$

h : Characteristic mesh size

$\overline{I}$: Stress Invariants

k : Turbulent kinetic energy $[m^2/s^2]$

N : Number of mesh elements

P : Pressure [kPa]

p : Order of convergence

P_f : Fuild pressure [kPa]

P_s : Solid pressure [kPa]

R_{fs} : Phase interaction term

Re : Reynolds number

S_p : Surface of particle [m^2]

$\overline{S}$: Strain rate [s^-1]

T : Temperature [K]

t : time [s]

u : Instantaneous velocity [m/s]

$\vec{u_s}$: Solid hase velocity

u_t : Settling velocity [m/s]

V : Volume of particle [m^3]

Greek Letters

α_s : Volume fraction

δ : Kronecker-Delta operator

ϵ : Kinetic energy dissipation rate [m^2/s^3]

η : Efficiency

λ_s : Solid bulk

μ : Dynamic viscosity of fluid [Pa.s]

μ_b : Dynamic viscosity for the bulk of fluid [Pa.s]

μ_w : Dynamic viscosity of fluid at wall [Pa.s]

μ_s : Shear viscosity [Pa.s]

ρ : Density $[kg/m^3]$

ρ_s : Density of particle $[kg/m^3]$

ρ_f : Density of fluid $[kg/m^3]$

τ : Viscous stress tensor

$\vec{\vec{\tau_s}}$: Solid stress tensor $[N/m^2]$

Φ_{ext} : Extrapolated value

Contents

Chapter 1

Introduction

Water treatment is a process that improves the water's quality to make it cleaner and more appropriate for end-use. This process can be used to obtain drinking water, irrigation, industrial water supply, river flow maintenance, water recreation, or different type of usage, including safe return to the environment. Water treatment aims to remove contaminants, undesirable components, and impurities or reduces their concentration to make the water suitable for the aimed end-use. Water treatment has a critical importance for human health. Also, allows them to use water for both drinking and watering the fields and sedimentation is one of the most important processes for water treatment [1].

Sediment is the silt, clay, loose sand, and other soil particles that settle at the bottom of a body of water over time. They can have different size ranges such as peddle structure, granular structure, etc. Sedimentation is defined as the separation process between solids and liquid volume. During the process, solids are separated from the liquid by settling down. Solids settle down at the bottom of a surface. For the water treatment, it is called a sedimentation tank. At this process, heavier impurities present in the liquid settle down at the bottom of the sedimentation tank due to its weight. The types of sedimentation tanks can be seen down below in Figure 1.1, 1.2, 1.3 [2].

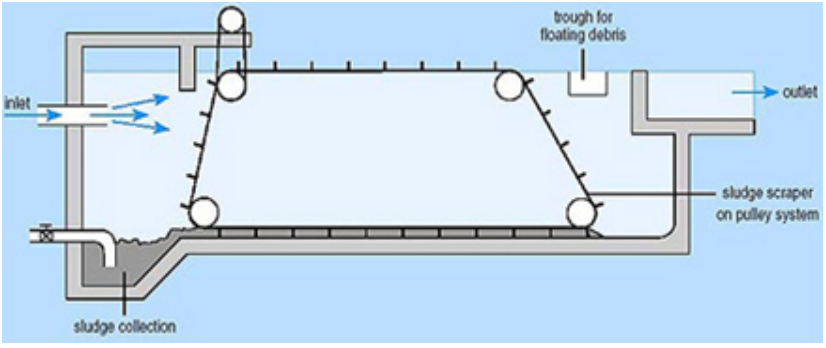

Figure 1.1: Rectangular horizontal flow tank[2]

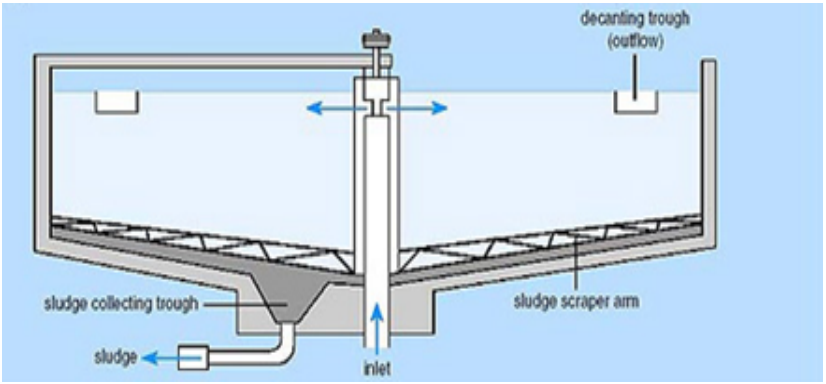

Figure 1.2: Circular, radial-flow tank[2]

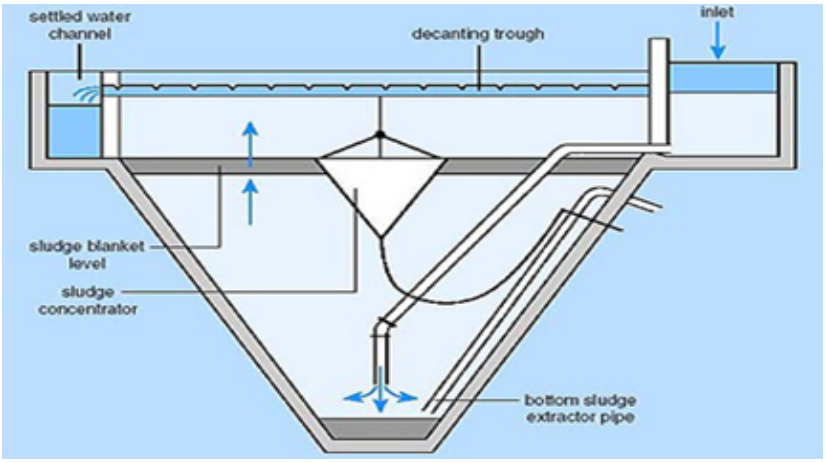

Figure 1.3: Hopper-bottomed, upward flow tank[2]

This process is called sedimentation and it takes some amount of time depending on the fluid's velocity or particle's size [3]. During this process, there is a limitation called terminal velocity for settling spherical particles. Terminal velocity is the maximum speed of an object that can reach during it falls through a fluid. The terminal velocity can be derived from the balances of several forces that affect those particles during the settling as seen in Figure 1.4[4].

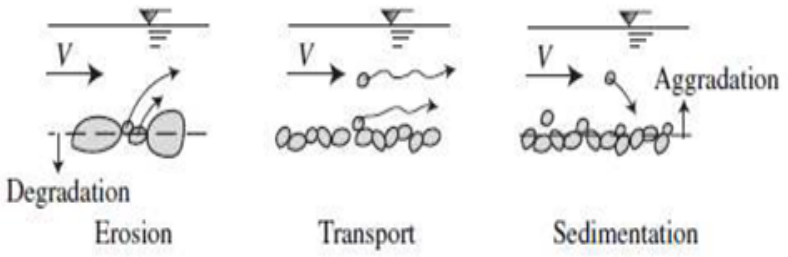

Figure 1.4: Processes of Erosion, Transport and Sedimentation [4]

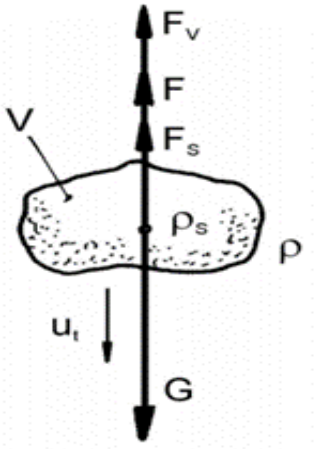

Figure 1.5: Forces acting on particles/moodle hydromechanical pro[5]

$$G - F_v - F_s - F = 0 \tag{1.1}$$

Gravitation force (G [N]) can be expressed as:

$$G = V\rho_s g \tag{1.2}$$

V: Volume of particle [m^3]
ρ_s: Density of particle [kg/m^3]
g: Gravitational force [m/s^2]

Buoyant force ($F_v[N]$) can be expressed as:

$$F_v = V\rho_f g \tag{1.3}$$

V: Volume of particle [m^3]
ρ_f: Density of fluid [kg/m^3]
g: Gravitational force [m/s^2]

Inertial force due to acceleration ($F_s[N]$) can be expressed as:

$$F_s = V\rho_s \frac{du_t}{dt} \tag{1.4}$$

V: Volume of particle [m^3]
ρ_s: Density of particle [kg/m^3]

Drag Force (F [N]) can be expressed as:

$$F = C_{Dt} S_p \frac{u_t^2}{2} \rho_f \tag{1.5}$$

C_{Dt}: Drag coefficient
S_p : Surface of particle [m^2]
u_t : Settling velocity [m/s]
ρ_f : Density of fluid [kg/m^3]

1.1 Multiphase Regime

Multiphase flow widely exists in many natural and industrial processes. It indicates the process where at least two states of materials flowing in a mixture at the same time. Multiphase flows can be divided into several categories including gas-liquid, gas-solid, liquid-solid, and so on according to the states of matter.

We can find the application of multiphase flows from a lot of industrial processes like power generation, process systems, and environment control. Facilities like steam generators, cooling towers, and steam turbines usually contain gas-liquid flows, a process like pneumatic conveying usually contains gas-solid flow, while hydro transport systems and water treatment processes usually contain the liquid-solid flow[6].

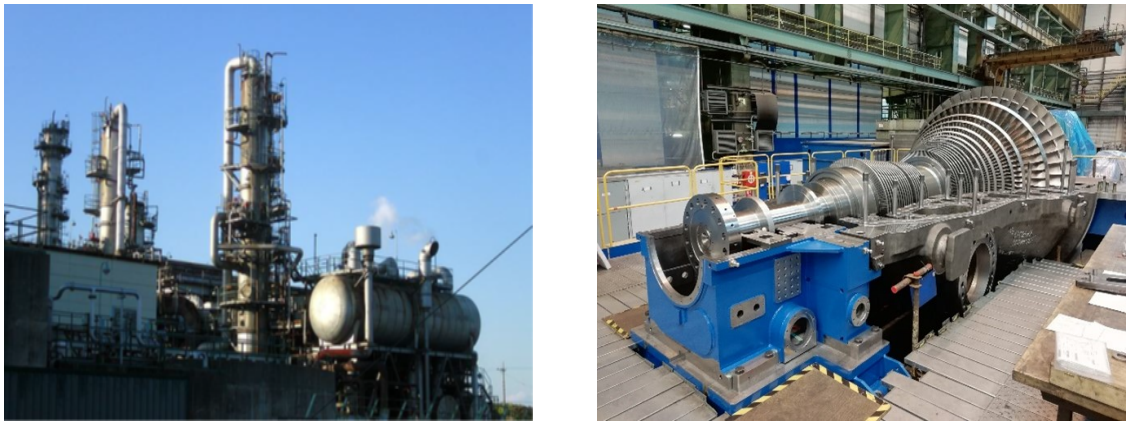

(a) (b)

Figure 1.6: Distillation Columns (Left) & Steam Turbine (Right)[7]

In this research, we focus on the process of sedimentation for water treatment, which is mainly a liquid-solid flow.

To study the multiphase flows, the basic and essential method is to establish a multiphase flow model and find the basic equations, by which we can analyse the pressure, velocity, temperature, apparent density, volume fraction, size, and distribution of suspended solids of each phase; and study the stability and criticality of multiphase flow state. The general methods accepted by the modern industry are a two-fluid model, homogeneous model, and statistical group model. Two- fluid model is used for situations

where the two-phase ratios are equivalent, the mathematical and physical equations of the single phases are established respectively, which considers the physical factors such as the resistance, relative displacement, momentum, mass, and heat exchange (transfer) between the phases. A homogeneous model is used for the two-phase mixed uniform flow, it can be generalized into a homogeneous (continuous medium) model and a diffusion model, and the classical hydraulics method is used for analysis. Statistical group model is mainly used for the two-phase flow of a group of particles (bubbles, droplets, and solid particles collectively referred to as particles), a statistical group (particle group) model is established by using random analysis.

Figure 1.7: Sewage Treatment Plant[8]

The core way of studying multiphase flow is to do the experimental measure of the physical model. For physical models, measurement technology is very important. Many new instruments and technologies have been applied in multiphase flow testing. For example high-speed photography, holography, flow display technology for observing flow patterns; laser flow meter (LDV), particle image velocimetry (PIV) for measuring speed; fiber optic sensor for detecting bubble concentration in liquid flow, the backpropagation(BP) neural network system for measuring the concentration of solid particles in the airflow; and the radioisotope method for measuring the average concentration of the section.

Even the physical model provides the most reliable experiment and results for practical use, the complexity of the experiment and the high cost of the advanced scientific facilities must be taken into account when studying such a process or designing related engineering equipment. Thus, for the first stage of this study, we will do the sedimentation model using CFD fluent.

1.2 CFD

Computational Fluid Dynamics (CFD) is a discipline that uses numerical methods to predict fluid flow behavior and solve mathematical equations that describe fluid flow by using laws of fluid mechanics. Therefore, it helps to study the spatial physical characteristics of steady fluid dynamics and the space-time physical characteristics of unsteady fluid dynamics. To solve these calculations, engineering software is used by defining boundary conditions, which then stimulates the flow of liquid and interaction with surfaces.

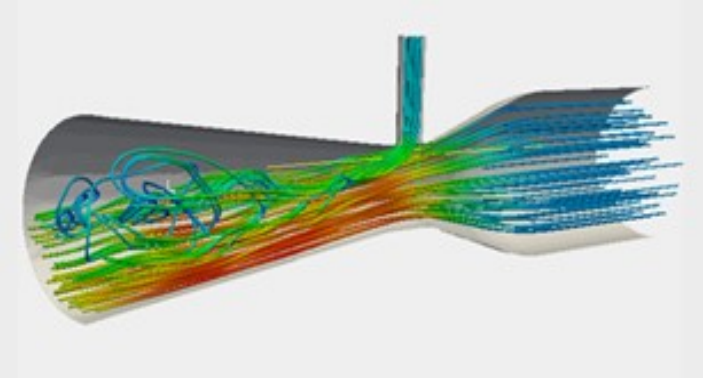

Figure 1.8: CFD visual example[9]

CFD is used by a wide variety of engineering problems and researches in many industries and studies such as aerodynamics analysis fluid flow, turbulence models, heat transfer and radiation, multiphase flows, from bubble columns to oil platforms, engine, and combustion analysis, etc.

To describe the physics of fluid flow mathematical equations are used. The continuity equation and the momentum equation, also known as the Navier-Stokes equation, and the energy equations are needed to describe the state of any type of flow and are generally solved for all flows in CFD, as seen in Equation 1.6, 1.13, 1.14.

1.2.1 Continuity equation

By applying the conservation of mass principle on a control volume fixed in space the continuity equation in conservation form can be obtained and it can be seen described differential form down below:

$$\frac{\partial \rho}{\partial t} + \nabla \cdot (\rho u) = 0 \tag{1.6}$$

where the "ρ" is the density of the fluid and u" is the velocity [m/s] at a point on the control surface, $u = f\ (\ x, y, z, t\ )$. For the incompressible flows, the simplified continuity equation can be expressed as:

$$\nabla \cdot \overrightarrow{u} = 0 \tag{1.7}$$

1.2.2 Momentum equation

The Navier Stokes equation is the application of Newton's 2nd law of motion to a fluid element that is fixed and expressed by three scalar equations that correspond to x,y,z axes over the conservation form of the momentum equation for the viscous flows.

The conservation form is described as:

$$\rho[\frac{\partial \vec{u}}{\partial t} + (\vec{u} \cdot \nabla)\vec{u}] = -\nabla p + \nabla \vec{\tau} + \rho \vec{g} \tag{1.8}$$

where g is the gravitational force $[m/s^2]$ and $\nabla\tau$ is the viscous stress tensor. The viscous stress tensor $\nabla\tau$ for Newtonian fluids is given in tensor notation as:

$$\tau_{ij} = \mu(\frac{\partial u_i}{\partial x_j} + \frac{\partial u_j}{\partial x_i} - \frac{2}{3}(\nabla \cdot u)\delta_{ij}) \tag{1.9}$$

The Kronecker-Delta operator "δ_{ij}" which is equal to 1 if $i = j$, else it equals to zero, x_i states one another perpendicular coordinate directions and μ is the dynamic viscosity.

The Navier-Stokes equation in terms of three scalar axes can be described as:
The momentum equation for x-axis:

$$\frac{\partial(\rho u_x)}{\partial t} + \nabla(\rho u_x u) = -\frac{\partial p}{\partial x} + \frac{\partial \tau_{xx}}{\partial x} + \frac{\partial \tau_{yx}}{\partial y} + \frac{\partial \tau_{zx}}{\partial z} + \rho g_x \tag{1.10}$$

The momentum equation for y-axis:

$$\frac{\partial(\rho u_y)}{\partial t} + \nabla(\rho u_y u) = -\frac{\partial p}{\partial y} + \frac{\partial \tau_{xy}}{\partial x} + \frac{\partial \tau_{yy}}{\partial y} + \frac{\partial \tau_{zy}}{\partial z} + \rho g_y \tag{1.11}$$

The momentum equation for z-axis:

$$\frac{\partial(\rho u_z)}{\partial t} + \nabla(\rho u_z u) = -\frac{\partial p}{\partial z} + \frac{\partial \tau_{xz}}{\partial x} + \frac{\partial \tau_{yz}}{\partial y} + \frac{\partial \tau_{zz}}{\partial z} + \rho g_z \tag{1.12}$$

Equation 1.10, 1.11, 1.12 are the Navier-Stokes equations in conservation form. For the incompressible fluids the second term of "τ" given in Equation 1.13 is zero due to the incompressibility constraint given in Equation 1.7. For a constant viscosity, the

Navier-Stokes equation for the incompressible fluids can be seen down below:

$$\rho[\frac{\partial \vec{u}}{\partial t} + (\vec{u} \cdot \nabla)\vec{u} = -\nabla P + \mu \nabla^2 \vec{u} + \rho \vec{g} \tag{1.13}$$

1.2.3 Energy equation

The energy equation is a mathematical statement that express the conservation of energy principle. For the incompressible flows, it can be seen down below:

$$\rho c_\mu \frac{\partial T}{\partial t} + \rho c_\mu u_i \frac{\partial T}{\partial x_i} = -P \frac{\partial u_i}{\partial x_i} + \lambda \frac{\partial^2 T}{\partial x_i^2} - \tau_{ij} \frac{\partial u_j}{\partial x_i} \tag{1.14}$$

1.3 Multiphase Modeling in CFD Fluent

Computational Fluid Dynamics (CFD) is an engineering tool that predicts fluid flow behavior by numerical simulations. CFD can resolve many types of flows by describing basic equations and flow models. This work focused on the simulation of sedimentation, which is a multiphase flow problem, there are several approaches for multiphase flow CFD modeling in ANSYS Fluent. In this research, multiphase particle flows are studied.

1.4 Overview

After giving basic information and describing few of the related topics about this work. In this section the information about the following steps will be given.

In this thesis the work has been divided into several parts, these parts can be seen down below;

a) Description of the fundamentals of the preliminary case and, obtain necessary data to start to define the first setup for the CFD analysis which will be carried out by ANSYS 2020 R1 software with a student license.

b) Finding an optimal Multiphase model to compare the results with the existing geometry, various analyzes will be run on ANSYS 2020 R1 software with different time steps and total time.

c)After obtaining the necessary data from the analyzes, Grid Convergence Index (GCI) will be used to utilize the time step.

d)As the following step, similarity analysis will be done and data will be compared with real experimental data to approve that different sizes of particles could be used for the following analyzes.

e)The geometry of the existing equipment will be used for the analyzes to compare the flow rate and the incline angle's effect on the lamella clarifier. Conclusions and recommendations will be made for further studies.

Chapter 2

Modeling Approaches

There are two basic approaches for multiphase flow modeling. Euler-Euler and Euler-Lagrange approach[10]. The Euler-Euler is a homogeneous approach and phases are interpenetrating one another. Volume fractions, as well as other phasic, are solved for both the phases are also solved at these control volumes. It can be used to compute any multiphase flow regime if and only if adequate closure relation is provided but it's not able to resolve details below grid size level.

In the Euler-Lagrange approach, individual particles are marked. The carrier phase obeys continuum conservation equations and the particle phase underlies Newton's 2nd law of motion. The physical laws apply directly to each particle and particles interact with the continuous carrier phase. The concept of particle parcel is tracking a representative number of physical particles, but it's limited to low particle number density. A general overview of modeling approaches can be seen in the table below:

Model	**Numerical Approach**	**Particle Fluid Interaction**	**Particle Particle Interaction**	**Particle Size Distribution(PSD)**
DPM	Fluid-Eulerian Particles- Lagrangian	Empirical models for subgrid particles	Neglected	Easy to include PSD because of Lagrangian description
DDPM - KTGF	Fluid-Eulerian Particles- Lagrangian	Empirical models for subgrid particles	Approximate P-P Interactions determined by granular models	Easy to include PSD because of Lagrangian description
DDPM - DEM	Fluid-Eulerian Particles- Lagrangian	Empirical models for subgrid particles	Accurate determination of P-P Interactions	Easy to include PSD because of Lagrangian description
Macroscopic Particle Model	Fluid-Eulerian Particles- Lagrangian	Interactions are determined as part of solution; particles span many fluid cells	Accurate determination of P-P Interactions	Easy to include PSD: if particles become smaller than the mesh,uses an empiricial model
Euler - Granular Model	Fluid-Eulerian Particles-Eularian	Empirical models for subgrid particles	P-P Interactions modeled by fluid properties such as granular pressure, viscosity, drag,etc.	Difference phases to account for a PSD; when size change operations happen use population balance models

Table 2.1: Overview of Modeling Approaches in ANSYS Fluent [10]

2.1 Description of Case and Preliminary Considerations

Sedimentation of small particles represents a dispersed multiphase flow, for that reason this case study focused on the Euler-Granular model and DDPM-KTGF model. The model's geometry is 180mm x 26mm size rectangle as seen in Figure 2.1. The analysis had been done for different total time and various time steps for the time step analysis to comparing the error size.

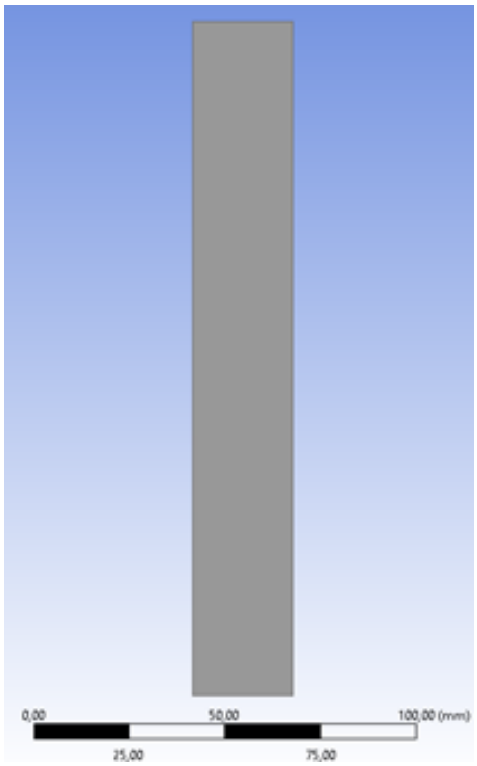

Figure 2.1: Model Geometry

For preliminary consideration, sedimentation time is estimated by using MATLAB script. The script and result can be seen down below for 0.1 mm chalk particle.

```
function [] = u3()

rho = 998.2;
mu = 0.001003;
nu = mu/rho;
rhos = 2560; dp = 1e-4; % chalk

drho = rhos - rho

```

```
Fg(dp,drho)
FCd(dp,1,nu,rho)

% function describing balance between gravity and drag forces
fun = @(u) Fg(dp,drho) - FCd(dp,u,nu,rho);
us = fzero(fun, [1e-11, 10])     % terminal settling velocity
Res = us*dp/nu
%fun(us)

dp
%4/3*(dp/2)^3/(dp)^3

H = 0.18;
t = H/us        % time for sedimenting the particle from top to bottom
dx = 0.001;     % characteristic size of mesh cell
dt = dx/us/3    % estimated time step

return

function y = Fg(dp,drho)  % gravity/buoyant force
g = 9.81;
y = 4*pi*((dp/2)^3)/3*drho*g;

function y = FCd(dp,u,nu,rho)  % drag force
re = u*dp/nu;
Sp = pi*dp^2/4;
%Cd = trans2(re);
Cd = fCd(re);
y = Cd.*Sp*rho.*u.^2/2;

function y = fCd(re)  % drag coeff.
N = length(re);
y = zeros(1,N);
for i=1:N
  if ( re(i) < 1 )
    y(i) = 24/re(i);
  elseif ( re(i) < 1000 ) % transient region 1 < Re < 1000
    y(i) = 24/re(i)*(1+re(i)^(2/3)/6);
  elseif ( re(i) < 2e+5 )  % turbulent region 1000 < Re <  2.10^5
    re(i) = 0.44;
  else
    re(i) = 0.19;
  end
end

%%%%%%%%%%%%%%%% Result %%%%%%%%%%%%%%%%
H_m  =

    0.18
```

```
dp_mm=

   1.0000e-04

t_s =

   21.2105
```

The sedimentation time of 0.1 mm diameter chalk particles for 0.18 m, was calculated as 21.718 seconds. According to that value, further analyzes had performed for 1-3-5 seconds total time and 0.001-0.005-0.01-0.02-0.04 second time step.

Chapter 3

Preliminary Analyzes & Grid Convergence Index

3.1 Model and Meshing

For modeling and meshing, ANSYS software has been used. The initial 2D model representing a water column was created as a 180mm x 26mm rectangle, and the generated mesh is depicted in Figure 3.1.

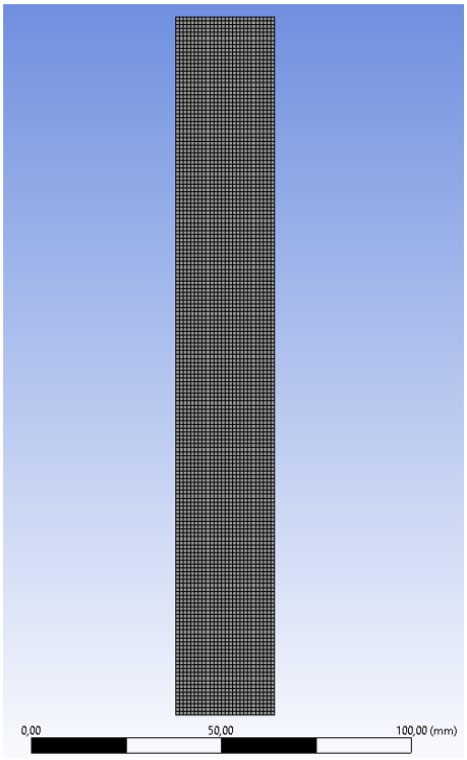

Figure 3.1: Model & Mesh

During meshing, element size was defined as 1mm. Hence, the generated total number of nodes and elements can be seein in Table 3.1:

Nodes	4887
Elements	4680

Table 3.1: Nodes & Elements

3.1.1 Mesh

The accuracy of the result in CFD analysis depends on the quality of the generated mesh. To create a quality mesh continuous geometric space must be divided into the right number of discrete elements of suitable size[11]. Mesh metrics available in ANSYS Meshing include:

· Element Quality
· Aspect Ratio
· Jacobean Ration
· Warping Factor
· Parallel Deviation
· Maximum Corner Angle
· Skewness
· Orthogonal Quality

The mesh quality for a simple rectangular geometry is close to perfect. This means according to skewness, It's close to 0 and orthogonal quality, It's close to 1.

3.2 Model Approach Setup

As mentioned before, Euler-Granular model and Dense Discrete Phase Model – Kinetic Theory of Granular Flow (DDPM-KTGF) model were used during the analysis. The setup of these two models is described in this section. First, fluent launcher setup has been set for the models with 2D dimension and with double precision option on. A computer with CPU Intel Core i7-9750h @ 2.6 GHz with 6 core and 12 thread, 16 GB RAM, RTX 2070 Mobile has been used for analyses. As parallel option, 4 out of 6 cores have been used. GPGPUs are set as 0 since student license is not allowed to use GPU during the analysis. The whole setup can be see down below in Figure 3.2.

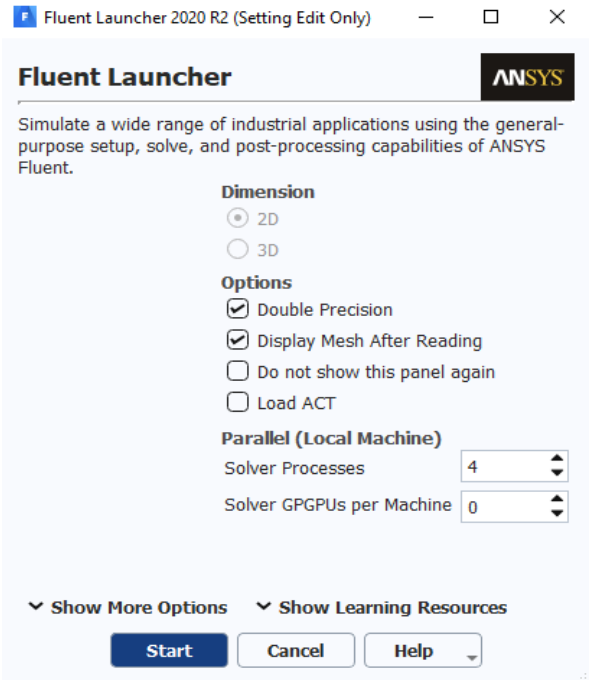

Figure 3.2: Fluent Launcher Setup - 2D Model

3.2.1 Euler-Granular Model

The Euler-Granular Model based on the kinetic theory of granular flow accounts for the effect of collisional particle-particle interactions. Solves set of conservation equations such as continuity, momentum, and energy which averaged equations can be seen from Equation 3.1, 3.2, 3.3.

Continuity equation[12]:

$$\frac{\partial}{\partial t}(\alpha_s \rho_s) + \nabla \cdot (\alpha_s \rho_s \overrightarrow{u_s}) = \dot{m}_{fs} \tag{3.1}$$

Where $\dot{m}_{fs}$ defines mass transfer.
Momentum equation[12]:

$$\frac{\partial}{\partial t}(\alpha_s \rho_s \overrightarrow{u_s}) + \nabla \cdot (\alpha_s \rho_s \overrightarrow{u_s} \overrightarrow{u_s}) = -\alpha \nabla p_f + \nabla \cdot \vec{\bar{\tau}}_s + \Sigma_{s=1}^{n}(\overrightarrow{R}_{fs} + \dot{m}_{fs}) + \overrightarrow{F_s} \tag{3.2}$$

$$\bar{\tau}_s = -P_s \bar{I} + 2\alpha_s \mu_s \bar{S} + \alpha_s(\lambda_s - \frac{2}{3}\mu_s)\nabla \cdot \overrightarrow{u_s} \bar{I} \tag{3.3}$$

$\bar{S} = \frac{1}{2}(\nabla \overrightarrow{u_s} + (\nabla \overrightarrow{u_s})^T)$ is the strain rate.

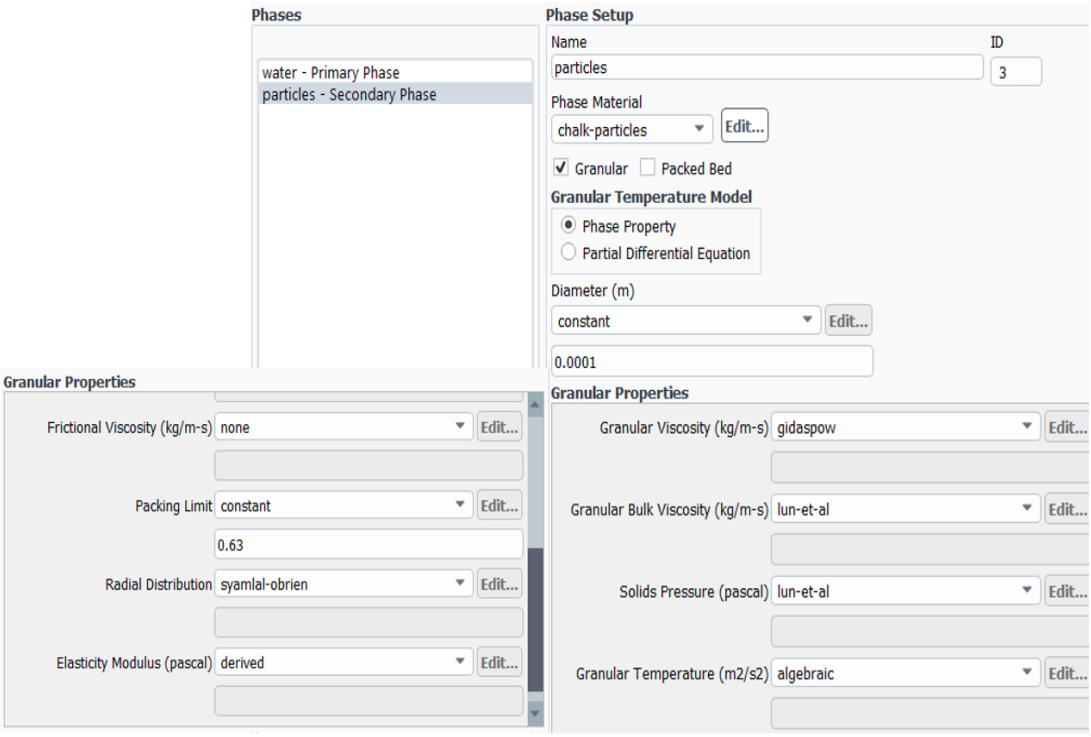

Figure 3.3: Secondary Phase Setup

Firstly, "gravity" activated and gravitational acceleration defined on the Y-axis as -9.81 m/s^2 and time chose as "Transient" in general settings. Since there is no flow to cause any turbulence in the geometry the viscous model was chosen as "Laminar" flow. The multiphase model was chosen as an inhomogeneous model "Eulerian" and the number of Eulerian phases is defined as two phases. Then chalk particles created and water added to the material list are both defined as fluids.

After these steps, the phase setup has finished as shown in Figure 3.3. Chalk-particles had been chosen as secondary phase material, the diameter was defined as 0.1mm. As granular viscosity "gidaspow" has defined [12], Lun et al. as granular bulk viscosity [12], Lun et al. as solid pressure [12].

Restitution coefficient is the reflection of the particles from each other, to reduce the reflection during sedimentation it's reduced from 0.9 to 0.1. can be seen in Figure 3.4.

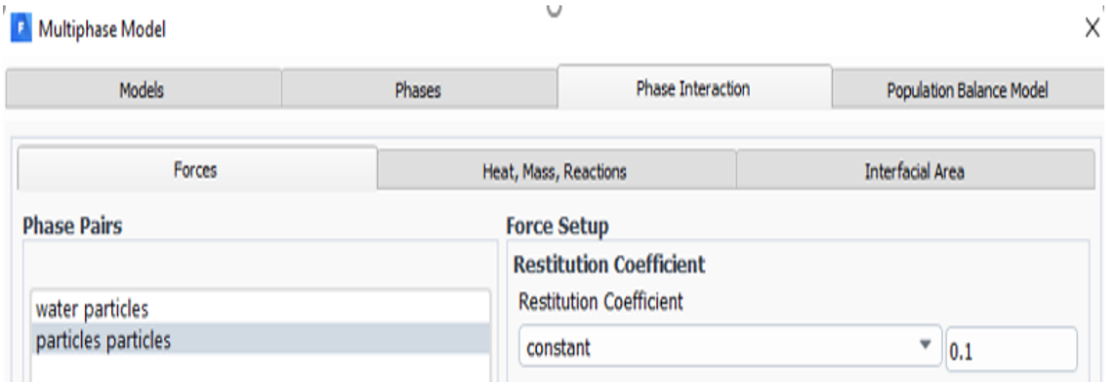

Figure 3.4: Restitution coefficient

The particle volume fraction was defined as 0.05, to have a 5% volume fraction from "Solution Initialization". Rest options are kept default. Last, a vertical line in the middle of the model geometry was created to obtain data for the further grid convergency index (GCI) which is also called time step analysis.

Results of the analysis can be seen in the Figure 3.6 for each total time.And the interface between pure water and particles' development by time, for each total time, can be seen on the Figure 3.5. The Euler model has a continuous phase hence there is a smooth dependency representing the interface between settled particles and pure water.

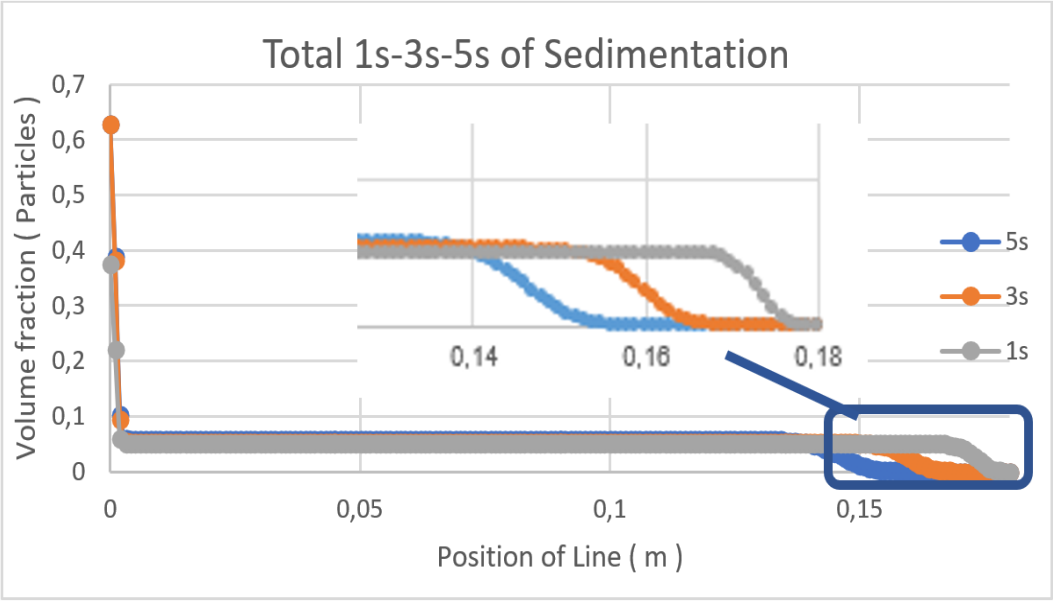

Figure 3.5: Packing limit by height

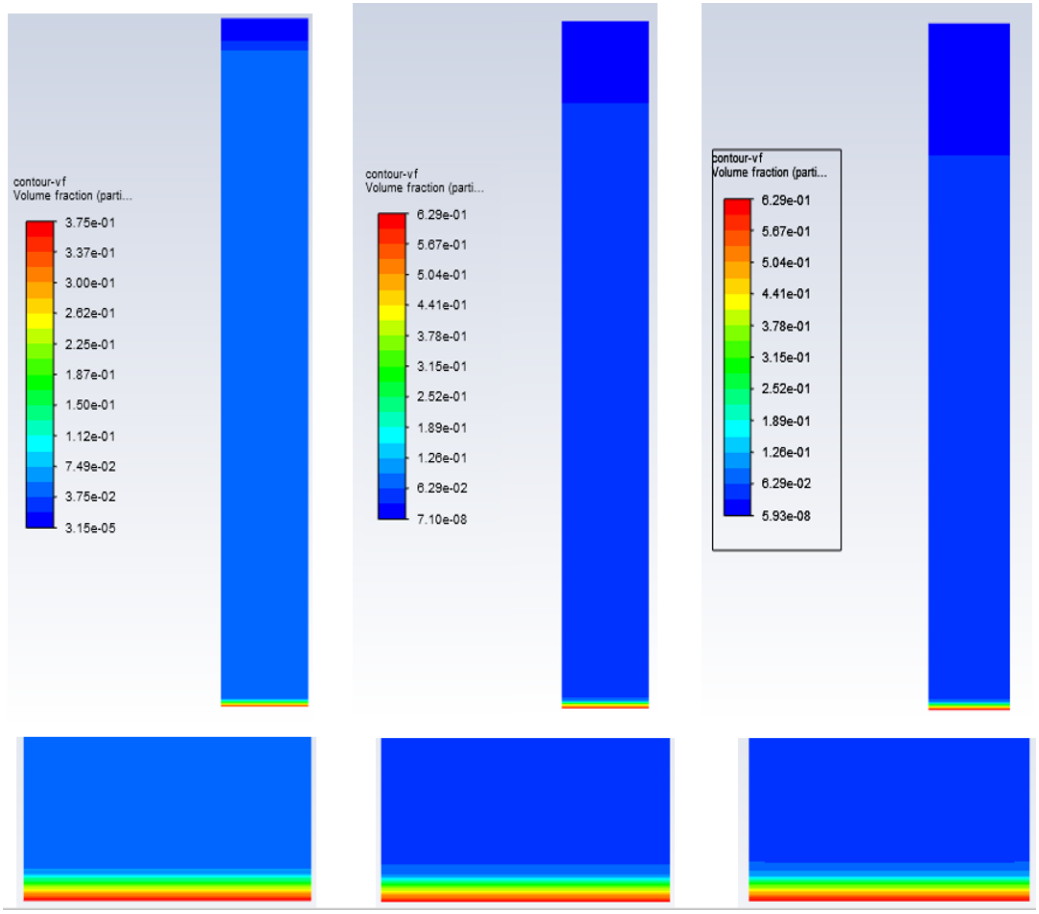

Figure 3.6: Contour of Volume fraction 1-3-5s

3.2.2 Dense Discrete Phase Model - Kinetic Theory of Granular Flow

The DDPM KTGF is a general framework in which the continuous phase is solved on an Eulerian grid and the particulate phase in a Lagrangian frame and it extends the application range of the Discrete Phase Model (DPM) from dilute to dense particulate flows. It accounts, the effect of volume fraction of particle phase, particle-particle interactions, fluid-particle coupling, and particle size distribution. DDPM-KTGF is suitable for dilute to moderately dense particulate flows, and faster computations due to the modeling of particle interaction effects. The solution procedure can be seen in Figure 3.7.

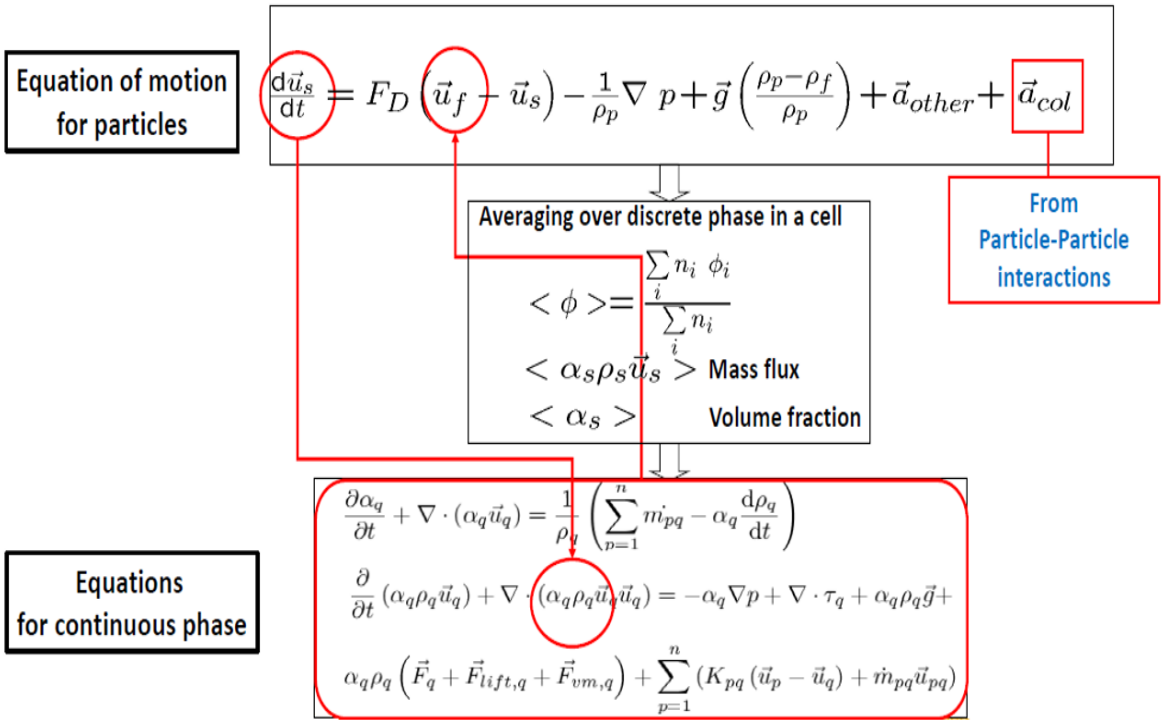

Figure 3.7: DDPM Solution Procedure[10]

The setup procedure has similarities with the Euler-Granular method, "Gravity" activated and gravitational acceleration defined value on the Y-axis is -9.81 m/s2, and time was chosen as "Transient" in general settings. Since there is no flow to cause any turbulence in the geometry the viscous model was chosen as "Laminar" flow.

The discrete phase was activated then the multiphase model was chosen as the inhomogeneous model "Eulerian" and the dense discrete phase model activated from Eulerian parameters. The number of eulerian phases is defined as 1 phase and the number of discrete phases is defined as 1. Then chalk particles are created in the material list as solid and water is added to the material list as fluid. After defining chalk as a solid, injection for DPM had been created. The setup of injection can be seen in Figure 3.8 down below.

Injection type was chosen to surface interior-surface_body and the material was chosen as chalk and discrete phase domain as phase-2. After that diameter of particles were defined and the total flow rate was calculated for 5% volume fraction as 600kg for 0.001s injection time as seen in Figure 3.8.

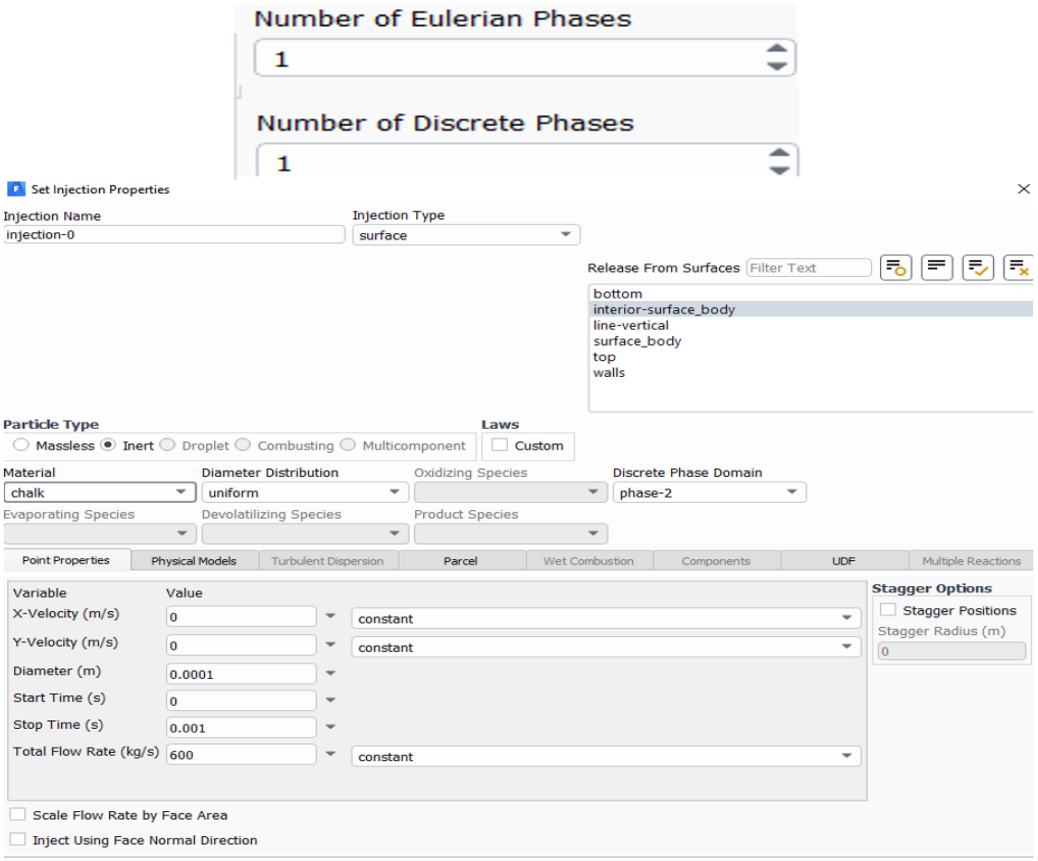

Figure 3.8: Injection Setup

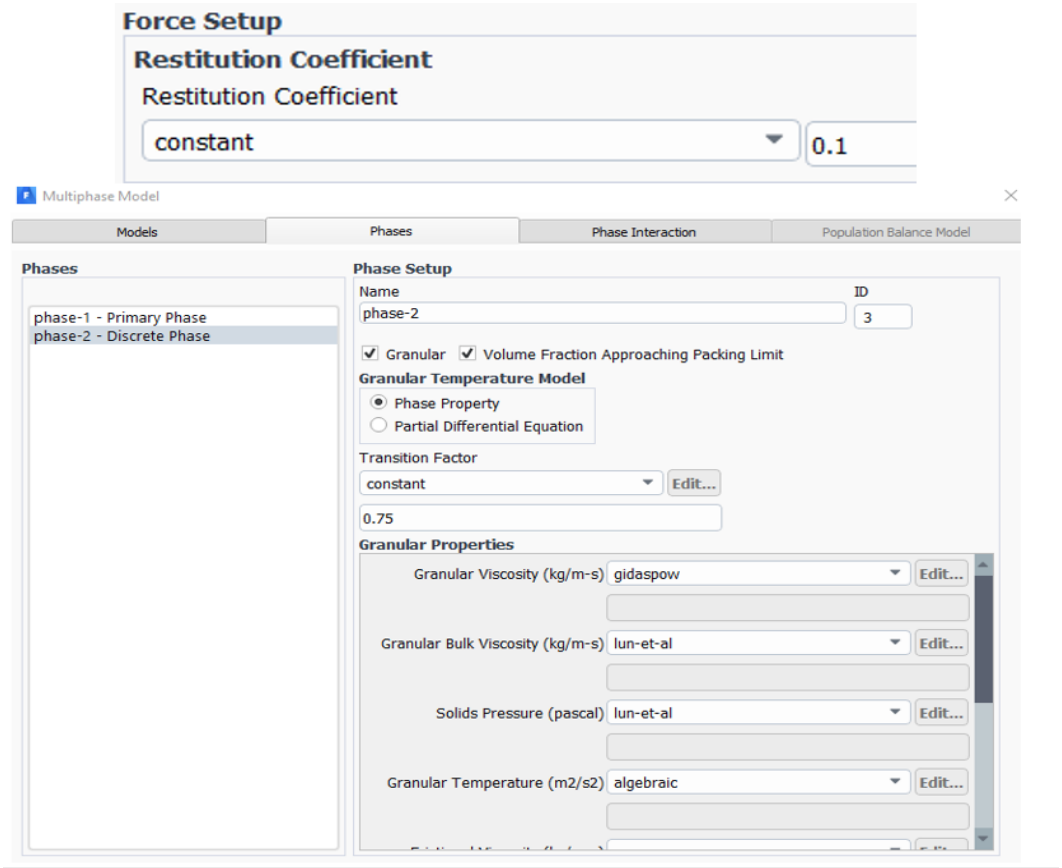

Figure 3.9: DDPM-KTGF Phase Setup

Phase setup is defined as the same with Euler-Granular model to compare results by using the same granular properties. Also, the restitution coefficient decreased from 0.9 to 0.1 too. Setup options can be seen in Figure 3.9.

Solution methods are set as default, and for the further time step analysis, a line is created in the middle of the geometry to obtain data of the interface between pure water and some particles, as seen in Figure 3.10.

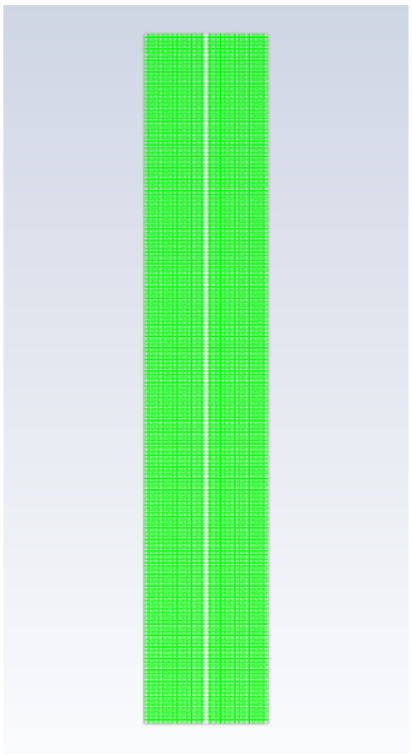

Figure 3.10: Created Line on the geometry

The result of volume fractions can be seen in the Figure 3.11,3.12 down below.

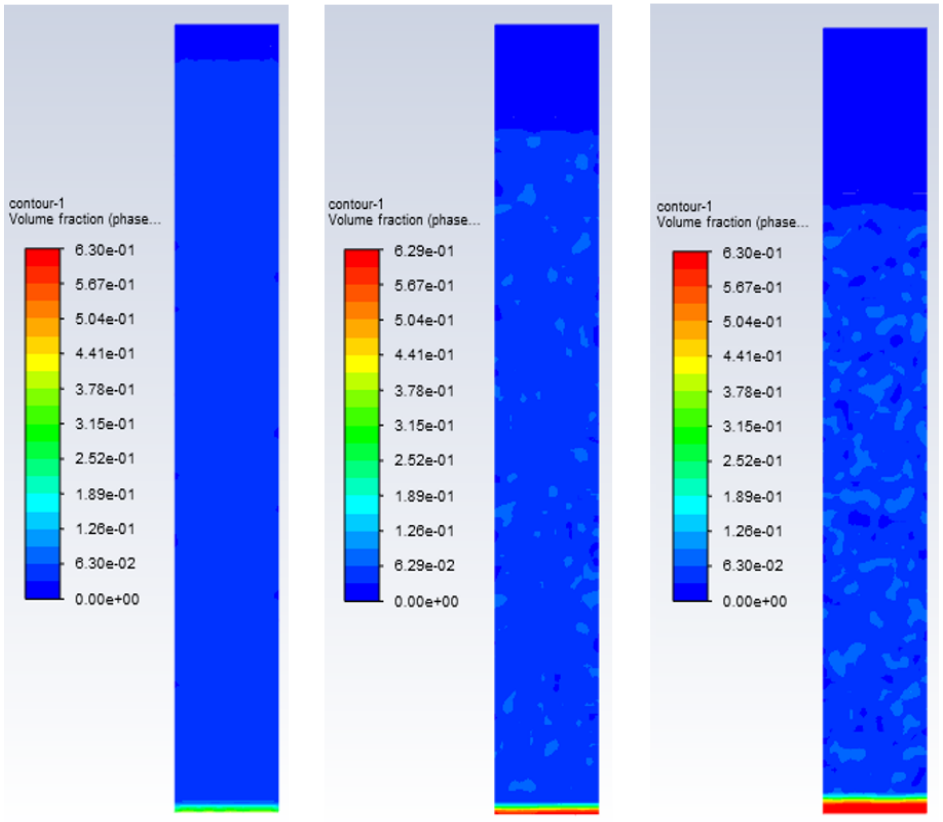

Figure 3.11: Volume fraction contour of 1-3-5s

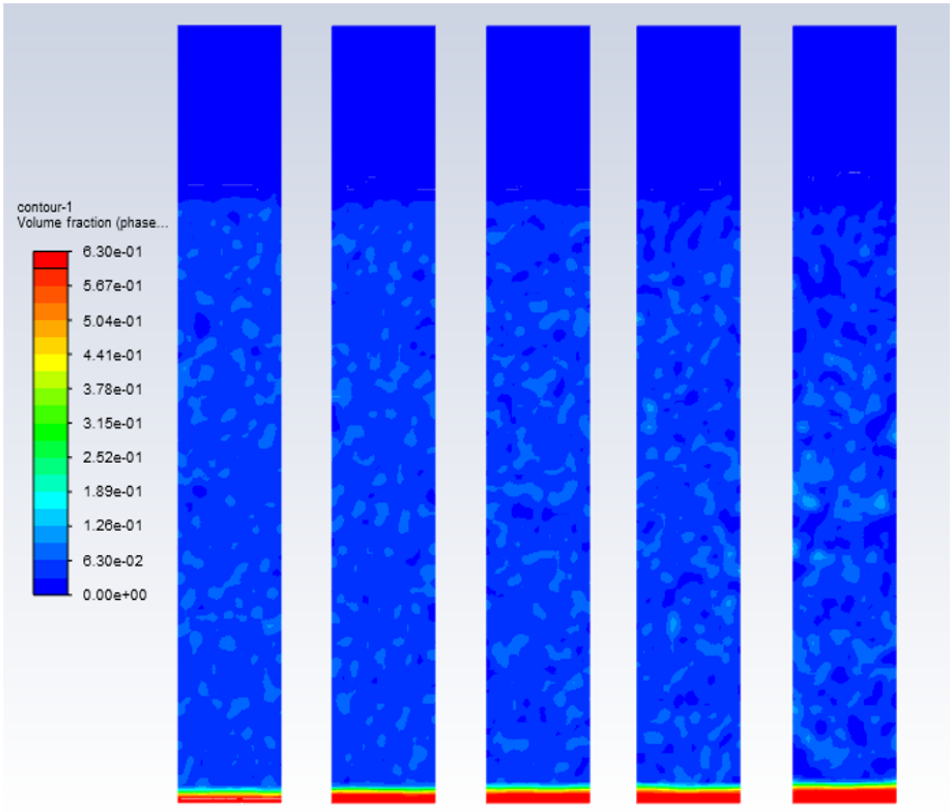

Figure 3.12: Volume fraction of 5 for each time step 0.04s-0.02s-0.01s-0.005s-0.001s

And the interface between pure water and particles' development by time, for each total time, can be seen in Figure 3.13. The average volume fractions from the obtained data for each time step from the Figure 3.13 are shown in Table 3.2:

Time step [s]	0.001	0.005	0.01	0.02	0.04
Average volume fraction	0.052036	0.052326	0.051849	0.052050	0.054600

Table 3.2: Average volume fraction of each time step

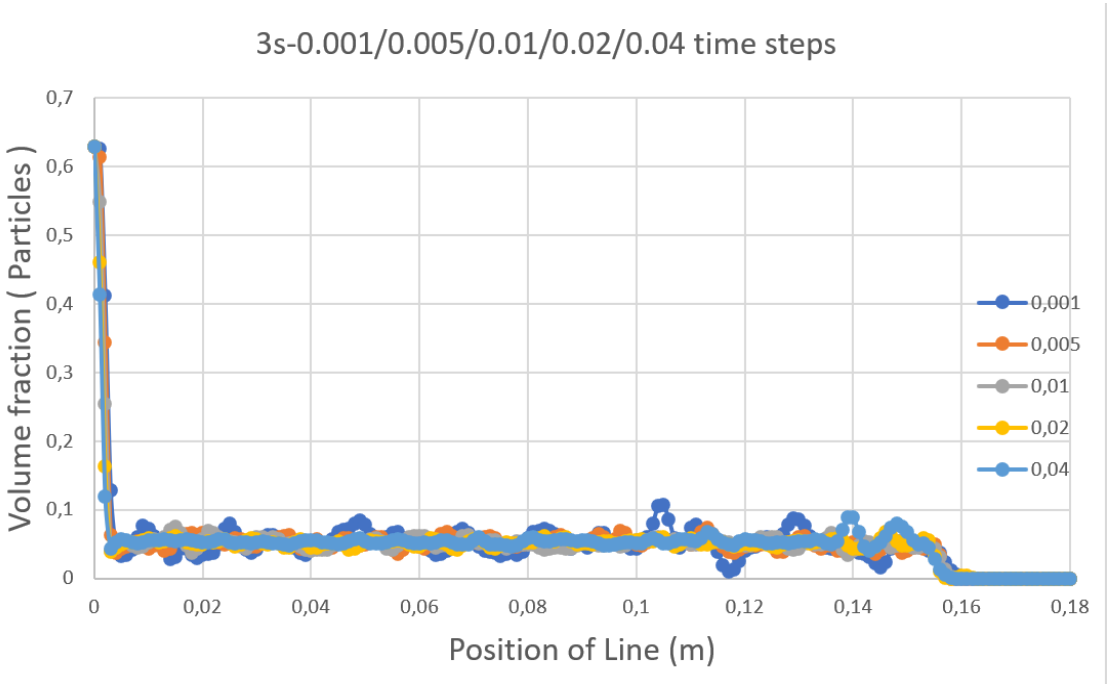

Figure 3.13: Packing limit by height

After creating more lines on the same geometry, a more smooth chart is obtained for the interface between pure water and particles which can be seen in Figure 3.14. Figure 3.15 and Figure 3.16 have been obtained as a chart of data from results of multiple lines analyzes with 0.05 mm particle size and 0.04 s time step for 20 s total time. The DDPM-KTGF model doesn't have a continuous phase for particles, hence volume fractions are not continuous.

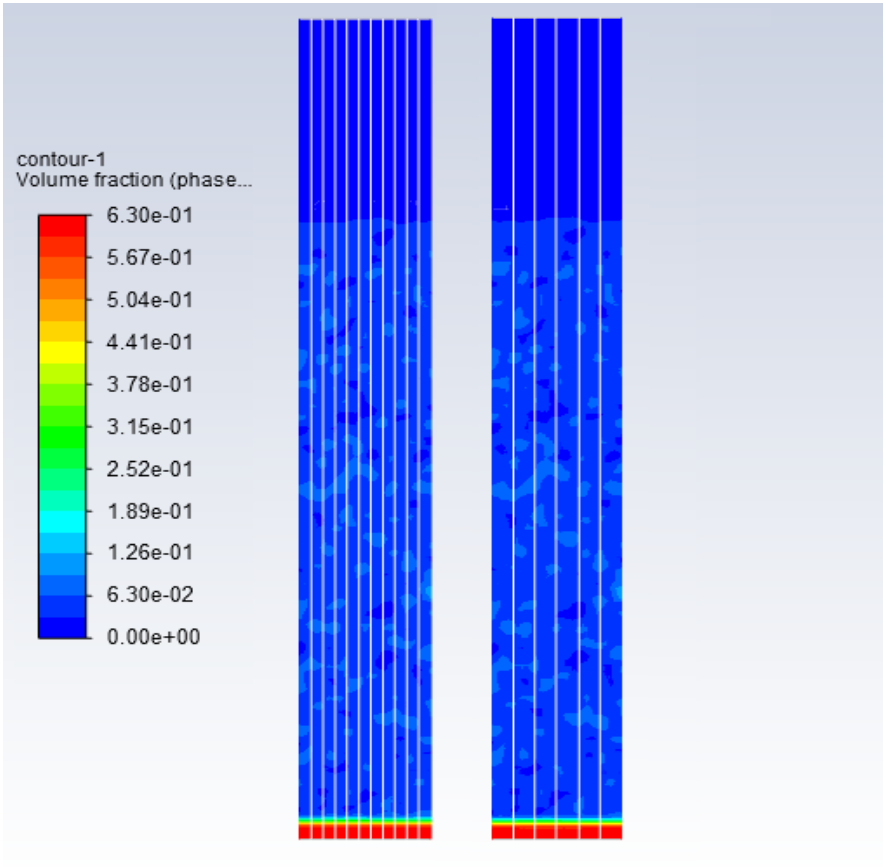

Figure 3.14: Created Surface Lines

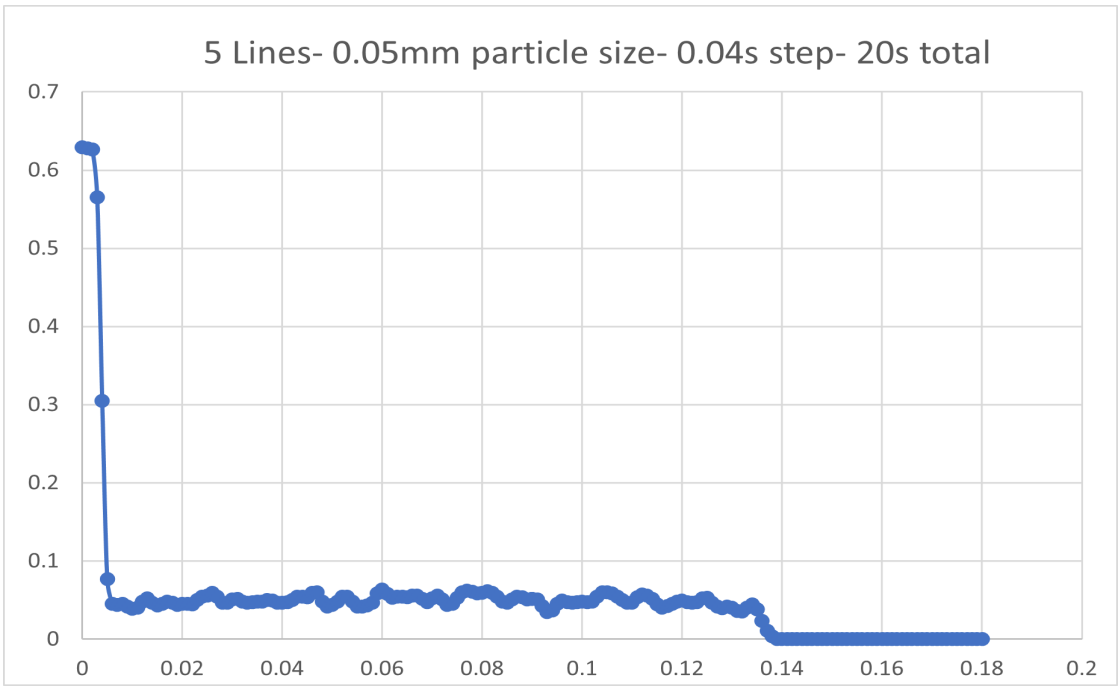

Figure 3.15: Packing limit by height - 5 Lines

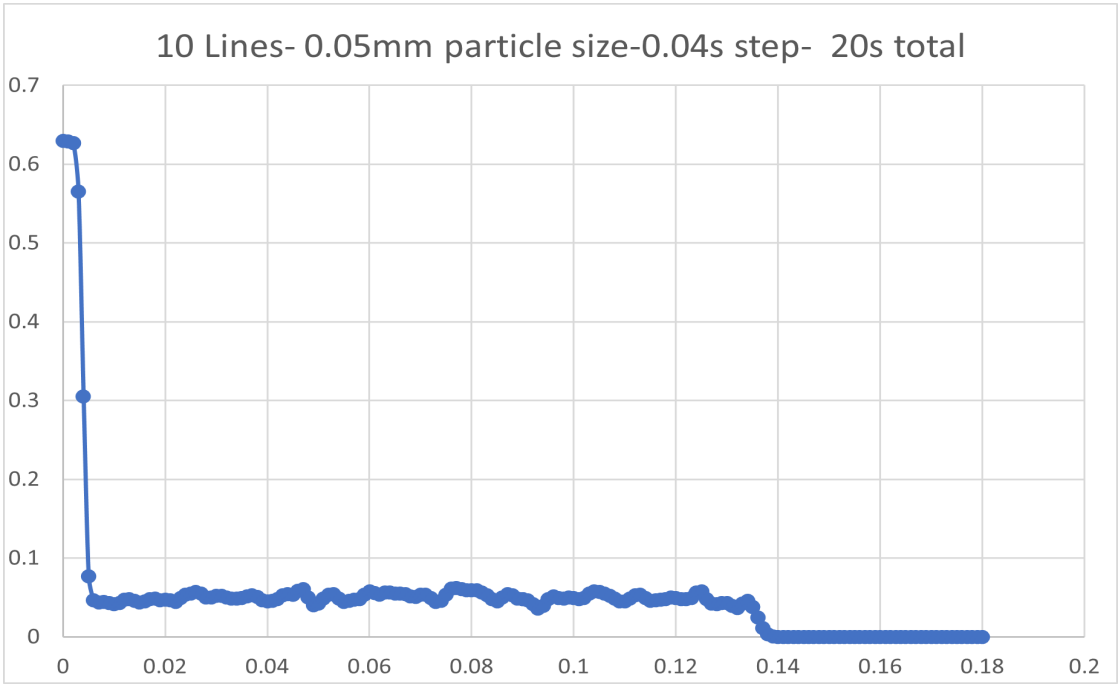

Figure 3.16: Packing limit by height - 10 Lines

As seen in Figure 3.17, the interface between pure water and settled particles is at the same position for both methods, Euler-Granular as well as DDPM-KTGF. But because of its discontinuity, it's difficult to find some quantity to evaluate GCI with DDPM-KTGF model. Therefore, the Euler-Granular method was used for the evaluation of GCI.

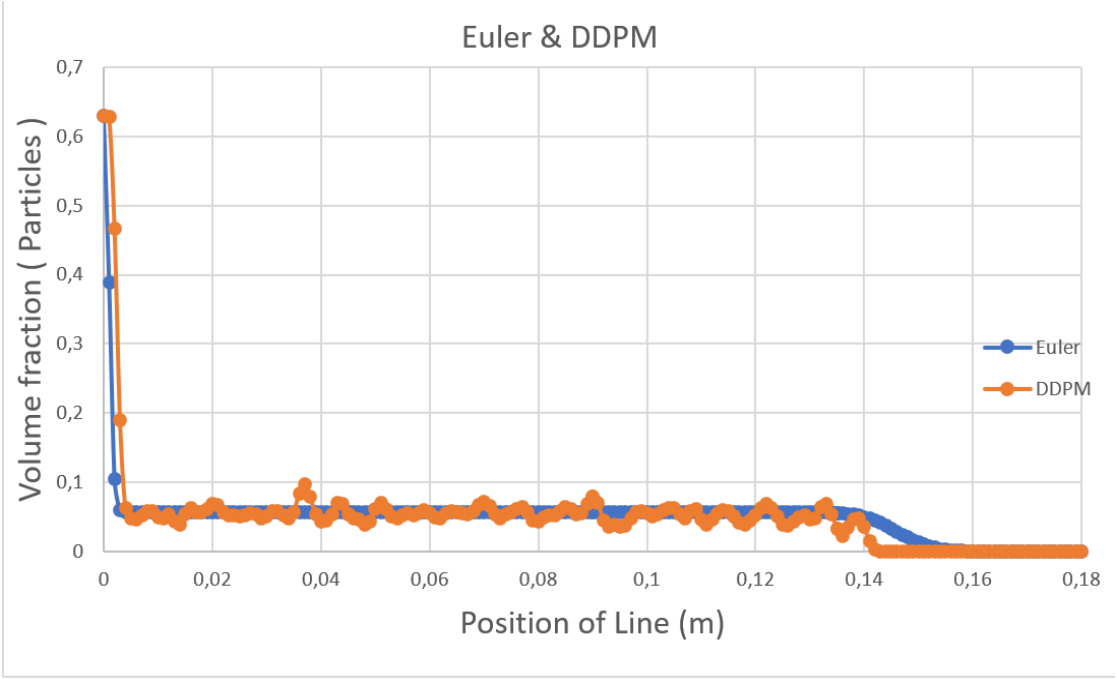

Figure 3.17: Packing limit by height Euler vs DDPM

3.2.3 Grid Convergency Index

Studying the spatial convergence of a simulation is a simple method for determining the sequential discretization error in a CFD simulation. It involves performing the simulation on two or more consecutive finer grids. When the grid is refined (as the grid cells become smaller and the no of cells in the flow domain increases) and the time step is refined (decreased), the spatial and transient discretization errors, respectively, should be asymptotically approach zero, excluding the computer rounding error.

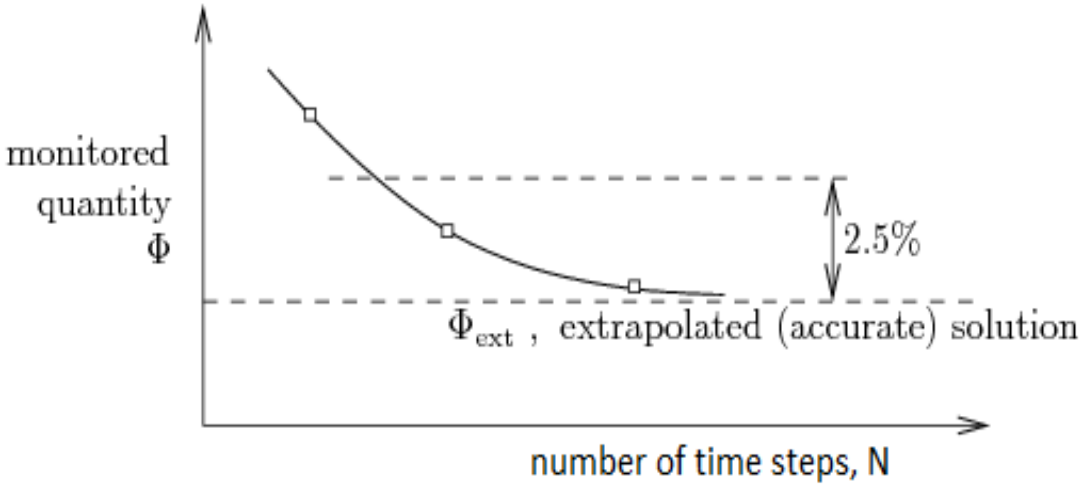

Figure 3.18: Grid Convergence Index Visual Chart[REF]

One of the methods to determine the GCI value of different levels of grids is developed by Roache[13], which is based on Richardson extrapolation[14]. GCI value of a certain grid-level indicates the inaccuracy of the obtained solution comparing to the real solution, in another word, the GCI value helps to check if the solutions are within the asymptotic range of convergence. In order to estimate the convergence accurately, three levels of the grid are usually applied, while the minimal two levels of grids are required to determine the GCI.

The dependency of solution on the number of grid cells can be described by the following equation:

$$\Phi = \Phi_{ext} + aN^{-\frac{p}{L}} \tag{3.4}$$

where Φ_{ext} represents the extrapolated value of the solution for infinitely large mesh size, a represents a model parameter, N represents the number of mesh elements, p is the order of convergence representing the solution accuracy, L equals 2 for 2D mesh and 3 for 3D mesh.

The three unknown parameters can be calculated from three equations for three different mesh sizes:

$$\Phi_1 - \Phi_{ext} - aN_1^{-\frac{p}{L}} = 0 \tag{3.5}$$

$$\Phi_2 - \Phi_{ext} - aN_2^{-\frac{p}{L}} = 0 \tag{3.6}$$

$$\Phi_3 - \Phi_{ext} - aN_3^{-\frac{p}{L}} = 0 \tag{3.7}$$

In terms of the average size of mesh elements, which equals the reciprocal value of the number of mesh elements, dependency of solution on element size is shown in Equation 3.8:

$$\Phi = \Phi_{ext} + ah^p \tag{3.8}$$

where h is the characteristic mesh size given by $h = -(\frac{1}{N})^{\frac{1}{L}}$ or $h = -(\frac{V}{N})^{\frac{1}{L}}$, V is the volume of cell. It can be observed from Equation 3.8 that, as the element size is decreased by increasing the number of mesh elements N, the solution approaches the extrapolated solution and for a theoretical case of h = 0, i.e $N \longrightarrow \infty$, the solution is the accurate solution equal to Φ_{ext}.

The three equations in terms of three different characteristic mesh sizes can be then written as:

$$\Phi_1 - \Phi_{ext} - ah_1^p = 0 \tag{3.9}$$

$$\Phi_2 - \Phi_{ext} - ah_2^p = 0 \tag{3.10}$$

$$\Phi_3 - \Phi_{ext} - ah_3^p = 0 \tag{3.11}$$

Subtracting those equations, we obtain:

$$\Phi_1 - \Phi_2 = ah_1^p[1 - (\frac{h_2}{h_1})^p] = ah_1^p(1 - r_{21}^p) \tag{3.12}$$

$$\Phi_2 - \Phi_3 = ah_2^p[1 - (\frac{h_3}{h_2})^p] = ah_2^p(1 - r_{32}^p) \tag{3.13}$$

where $r_{21}^p = \frac{h_2}{h_1}$ is refinement ratio for finest grid size, $r_{32}^p = \frac{h_3}{h_2}$ is refinement ratio for

mid-size grid level. Dividing the Equation 3.12 and 3.13 yields:

$$\frac{\Phi_1 - \Phi_2}{\Phi_2 - \Phi_3} = \frac{1}{r_{21}^p} \frac{1 - r_{21}^p}{1 - r_{32}^p} \tag{3.14}$$

The differences between particular variables can be written as:

$$\epsilon_{21} = \Phi_2 - \Phi_1, \epsilon_{32} = \Phi_3 - \Phi_2 \tag{3.15}$$

p can be separated from Equation 3.14 and it can be described as:

$$p = \frac{1}{lnr_{21}}[ln\frac{\epsilon_{32}}{\epsilon_2 1} + ln\frac{r_{21}^p - 1}{r_{32}^p - 1}] \tag{3.16}$$

This relation is similar to the equation published by Celik (2008)[15]:

$$p = \frac{1}{lnr_{21}}|ln|\frac{\epsilon_{32}}{\epsilon_2 1}| + q|, q = ln(\frac{r_{21}^p - s}{r_{32}^p - s}), s = sign\frac{\epsilon_{32}}{\epsilon_2 1} \tag{3.17}$$

The absolute values and the sign function are for situations in which there is non-monotonous increase or decrease of the monitored quantity (e.g. $\Phi_1 < \Phi_2$ and $\Phi_2 > \Phi_3$). The equation for p is solved numerically.

The parameter a can be expressed as:

$$a = \frac{\Phi_1 - \Phi_{ext}}{h_1^p} \tag{3.18}$$

and substituting the expression of a in Equation 3.10, we obtain:

$$\Phi_{ext} = \frac{\Phi_1 r_{21}^p - \Phi_2}{r_{21}^p - 1} \tag{3.19}$$

and the accuracy of Φ_1 solution for the finest mesh in terms of GCI is:

$$GCI_{21} = F_s \frac{\Phi_{ext} - \Phi_1}{\Phi_1} \tag{3.20}$$

where F_s is the factor of safety in the estimation of numerical accuracy. Substituting F_s of 1.25, we obtain a fine-grid convergence index:

$$GCI_{21} = \frac{1.25 e_a^{21}}{r_{21}^p - 1} \tag{3.21}$$

where $e_a^{21}$is the approximate relative error,

$$e_a^{21} = |\frac{\Phi_1 - \Phi_2}{\Phi_1}| \times 100[\%] \tag{3.22}$$

Similar relation for GCI of mid-size mesh can be written as:

$$GCI_{32} = \frac{1.25e_a^{32}}{r_{32}^p - 1} \tag{3.23}$$

It is recommended that the refinement ratios, r_{21}^p and r_{32}^pbe greater than 1.3, (Celik, 2008).

For this case study, GCI for the time step was evaluated by MATLAB script and function which can be seen below for 5s total time. For the 1s-3s total time same script and function were used[15].

```
function [ N, Phi, GCI ] = gci(N,Phi,D)
% grid convergence

format compact;

[N, i] = sort(N,'descend');
Phi = Phi(i);
GCI = zeros(3,1);

% Celik (1993)
%N = [ 18000, 8000, 4500 ]; Phi = [6.063, 5.972, 5.863];
N
Phi
%%h1 = sqrt(N1); h2 = sqrt(N2); h3 = sqrt(N3);
%r21 = sqrt(N(1)/N(2))
%r32 = sqrt(N(2)/N(3))

r21 = (N(1)/N(2))^(1/D)
r32 = (N(2)/N(3))^(1/D)
if ( r21 < 1.3 || r32 < 1.3 )
  disp('refinement factors r21 and r32 should be greater than 1.3');
end

eps32 = Phi(3)-Phi(2)
eps21 = Phi(2)-Phi(1)
R = eps21/eps32
s = sign(eps32/eps21)

fq = @(p) log((r21.^p-s)./(r32.^p-s));
fp = @(p) p - 1/log(r21)*abs(log(abs(eps32/eps21))+fq(p));
p = fzero(fp,1)
%p = fsolve(fp,1)

Phi21ext = (r21^p*Phi(1)-Phi(2))/(r21^p-1)
%%Phi32ext = (r32^p*Phi2-Phi3)/(r32^p-1)

e32a = abs((Phi(2)-Phi(3))/Phi(2))*100
```

```
%GCI32 = 1.25*e32a/(r32^p-1)
GCI32 = 1.25*abs(Phi21ext-Phi(2))/Phi(2)*100
e21a = abs((Phi(1)-Phi(2))/Phi(1))*100
e21ext = abs((Phi21ext-Phi(1))/Phi21ext)*100
%GCI21 = 1.25*e21a/(r21^p-1)
GCI21 = 1.25*abs(Phi21ext-Phi(1))/Phi(1)*100

asymptoticRange = GCI21*r21^p/GCI32

rs = (asymptoticRange*GCI32/1)^(1/p)

plot(N,Phi,'r*', N,Phi,'b', [0.9*min(N), 1.1*max(N)], [Phi21ext Phi21ext],'m');
grid on;

GCI33 = 1.25*abs(Phi21ext-Phi(3))/Phi(3)*100

GCI(1) = GCI21;
GCI(2) = GCI32;
GCI(3) = GCI33;

return

% for output graphics a-b-c%
t = 5
dt = [ 0.1 0.02 0.005  ]
Phi = [ 0.146057176988027 0.14578159003159 0.145725177304965 ]
N = t./dt

figure(2);
gci5s(N,Phi,1)
```

Since the Eulerian-Granular model has a continuous phase, it was able to evaluate GCI from the slope, as seen in Figure 3.5. The results of 1s-3s-5s GCI values from the figures down below where GCI33 express 0.1s time step error rate (in %), GCI32 express 0.02s time step error rate (in %), GCI21 express 0.005s time step error rate (in %), as seen in Figure 3.19.

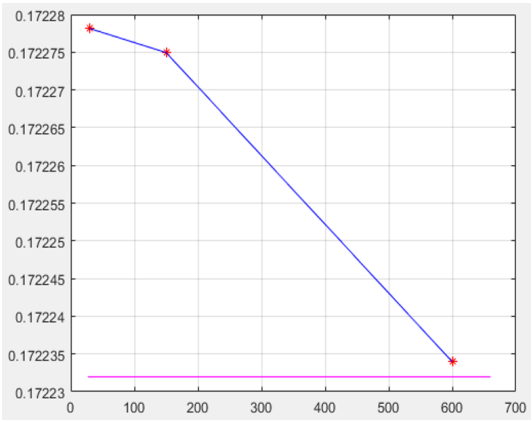

(a) total time 1s

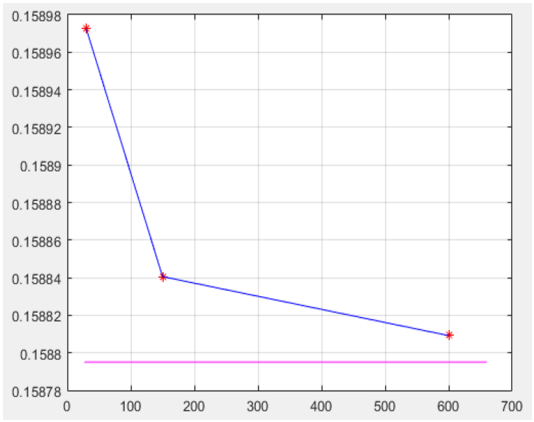

(b) total time 3s

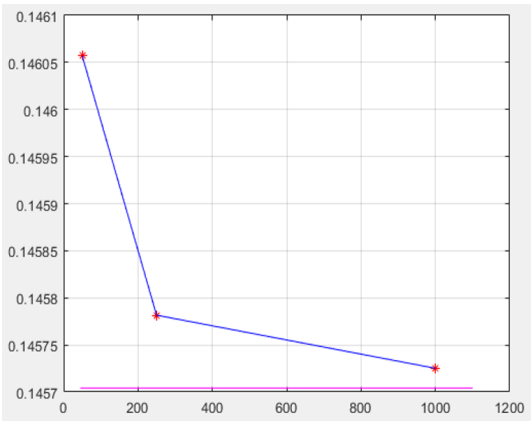

(c) total time 5s

Figure 3.19: GCI charts

Total Time	1s	3s	5s
Φ_1	0.172278142	0.158972453	0.146057176988027
Φ_2	0.171812221	0.158840545	0.14578159003159
Φ_3	0.171680781	0.158809176	0.145725177304965
Φ_{21ext}	0.1716	0.1588	0.1457
r_{21}	4	4	4
r_{32}	5	5	5
$e_{32a}(\%)$	0.2712	0.0830	0.1890
$e_{21a}(\%)$	0.0766	0.0198	0.0387
GCI32 (%)	0.0663	0.0357	0.0312
GCI21 (%)	0.0179	0.0111	0.0014
GCI33 (%)	0.3020	0.1394	0.0335

Table 3.3: Input and output values under different total time & time steps

After the GCI analysis, the values can be seen in Table 3.3. The numerical uncertain-

ties for 1s total time, 0.1s time step was found 0.3020%, 0.02 s time step as 0.0663% and 0.005s as 0.0179%. For the higher total times, the GCI values got lower.

In Table 3.3, It can be seen that when the total time increases the error rates are start to decrease. Hence, bigger time steps are being available to use for the longer analyzes. As a result of this GCI analysis, for further The Euler model analyzes, bigger time steps close to or even 0.1 s can be used.

3.3 Similarity analysis

In real apparatuses, much smaller particles are present which means that much larger settling times are observed. This would result in much longer simulation times and the computational requirements would increase substantially. So the aim was to perform simulations with larger particles which could be then recalculated to the situation with smaller particles. In this section, the sedimentation of the different sized particles will be compared according to the given equilibrium Equation 3.32. To approve that the results are close to each other and as the next step, real experimental data is needed to compare it with the obtained data from the first analyzes. After the comparison and approval of these obtained data, It's possible to use bigger particles for the following analyzes for the following case.

F_g defines gravitational forces on the particle. It can be expand as Equation 3.24:

$$F_g = mg = V_p \rho_p g = \frac{\pi d_p^3}{G} \rho_p g \tag{3.24}$$

F_d defines drag forces on the particle:

$$F_d = C_{Dt} S_p \rho_f \frac{u^2}{2} \tag{3.25}$$

where $C_{Dt} = \frac{24}{Re}$ is drag coefficient, for the stoke region $Re < 1$. Thus Equation 3.25 can be written as:

$$F_d = \frac{3\pi}{8} \mu d_p u \tag{3.26}$$

where μ dynamic viscosity is, d_p is diameter or particle.

$$F_b = V_p \rho_f g \tag{3.27}$$

In steady-state case Gravitational forces are equal to Buoyant and Drag forces the

equilibrium can be seen as Equation 3.28 :

$$F_g = F_b + F_d \tag{3.28}$$

Where u is:

$$u = \frac{d_p^2 \Delta\rho g}{18\mu} \tag{3.29}$$

and $\Delta\rho = \rho_p - \rho_f$

The equilibrium between two different particle sizes can be expressed as:

$$t_1 = \frac{L}{u_p} = \frac{L}{\frac{d_{p1}^2 \Delta\rho g}{18\mu}} \tag{3.30}$$

$$t_2 = \frac{L}{\frac{d_{p2}^2 \Delta\rho g}{18\mu}} \tag{3.31}$$

$$\frac{t_1}{t_2} = \frac{d_{p2}^2}{d_{p1}^2} \tag{3.32}$$

```
% similarity analysis

dp1 = 1e-4
dp2 = 5e-5
t1_t2 = (dp1/dp2)^2

t1 = 5
t2 = t1*(dp1/dp2)^2

% experiment figure ... 250 min
t1 = 250*60
dp1 = 2.85e-6  % chalk mean diamter
dp2 = 1e-4
t2 = t1*(dp1/dp2)^2 % simulation time for dp2 to get same position of the interface

%% RESULTS %%
dp1 =
   1.0000e-04
dp2 =
   5.0000e-05
t1_t2 =
     4
t1 =
     5
t2 =
    20
t1 =
       15000
```

```
dp1 =
   2.8500e-06
dp2 =
   1.0000e-04
t2 =
   12.1837
```

The simulation is applied for particle size of dp1 and dp2, the exact value can be seen in the Matlab script above. Theoretically, simulations of different particle sizes should obtain a similar position of the interface for the final time $t2 = t1 * (dp1/dp2)^2$. The first simulations are proceeded with the Euler model, for the 0.1mm and 0.05mm particle sizes. According to Equation 3.32 5s total time for 0.1mm particle size is equal to 20s total time for 0.05mm particle size and for the real experiment particle sizes total time for 0.1mm particle size is equal to 12.1837s.

3.3.1 Comparison between different particle sizes

To make the comparison between different particle sizes for both methods, the same model setups had been selected as in previous chapters. During this step, two different sizes of particles is used 0.1mm & 0.05mm with Euler Granular Model. The 0.05mm diameter particles' diameter setup can be seen down below:

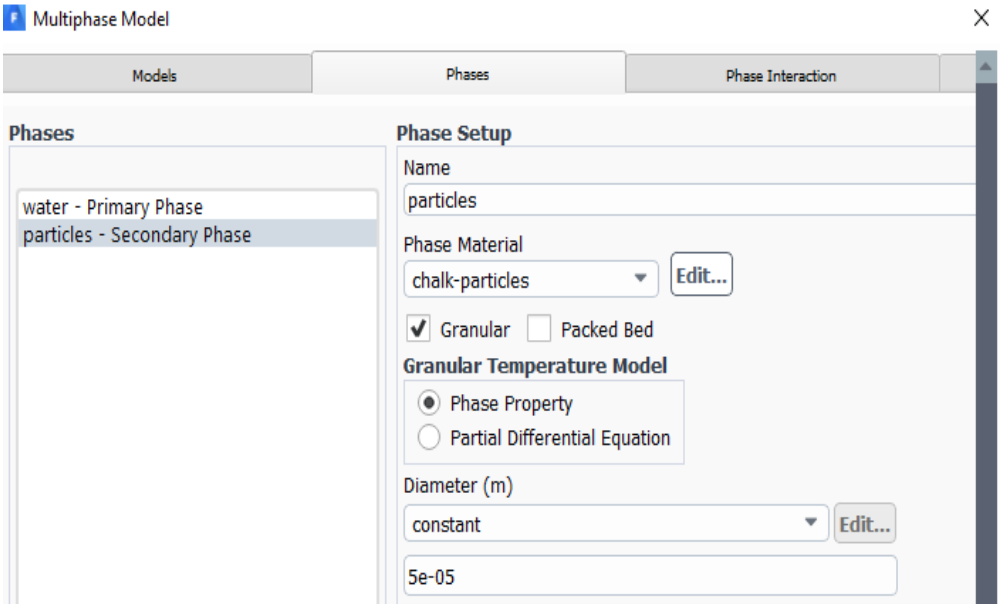

Figure 3.20: Defining 0.05mm diameter Particles Euler

To obtain an interface between pure water and particles the midline on geometry has been drawn like the previous chapter's Figure 3.10.

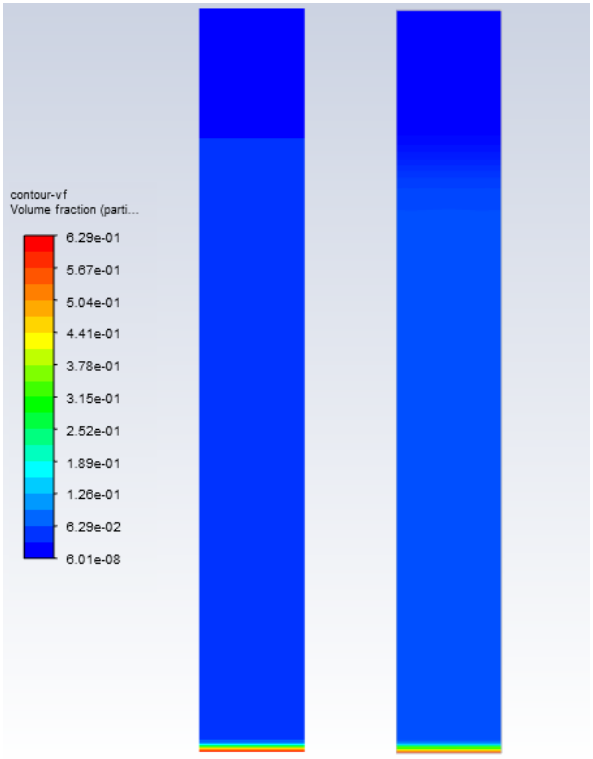

Figure 3.21: Euler model, 0.1mm 5s (left) vs 0.05mm 20s (right)

Figure 3.21 illustrates the volume fraction contour which has been obtained for the particles' after the analysis. Contour results are similar to each other which can be seen in the figure.

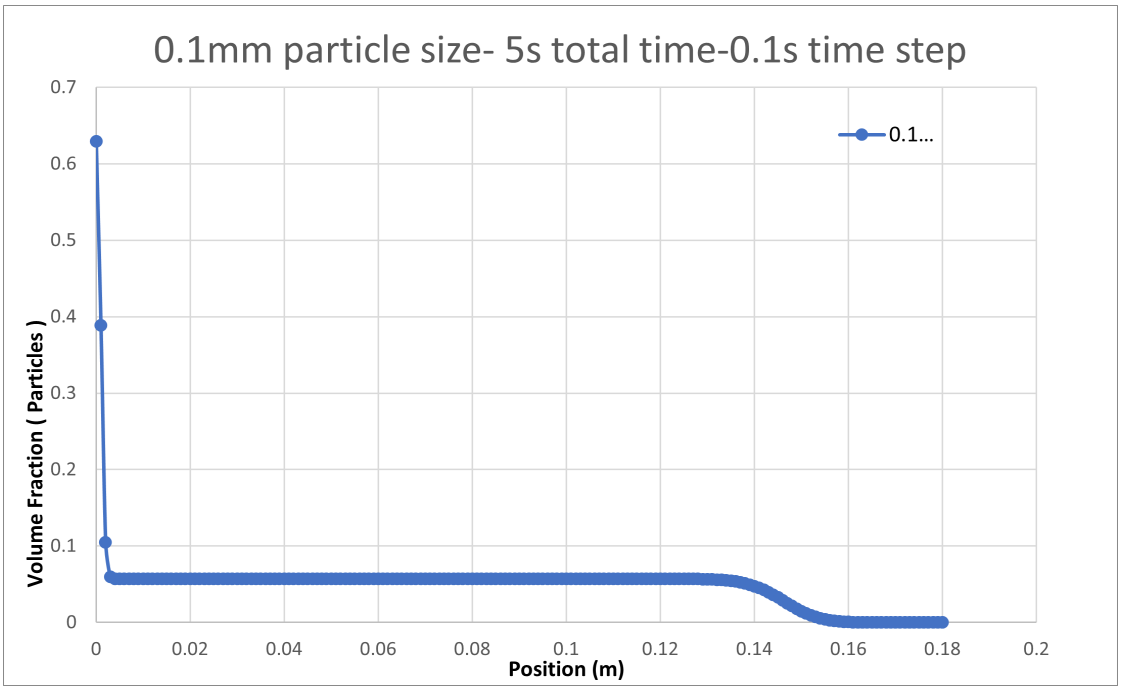

Figure 3.22: Euler model- 0.1mm particle size - 5s total time-0.1s time step

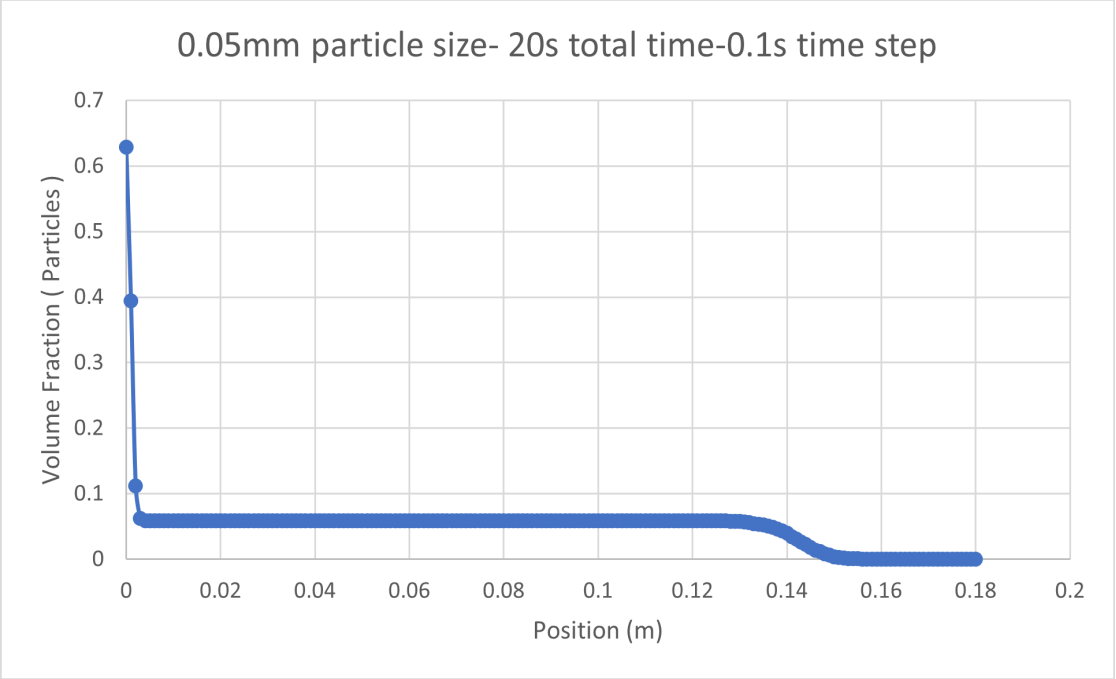

Figure 3.23: Euler model- 0.05mm particle size - 20s total time-0.1s time step

Figure 3.22 Figure 3.23 show interface between pure water and particles for different particle sizes as in Figure 3.21 above. The interface height is similar to each other, which is approximately 0.145m.

As a result of the Euler method comparison of the different sized particles, simulation with bigger particles does have practical meanings and it will be used for the following steps.

In the next step of this chapter, DDPM-KTGF model was used with two different sizes of particles, which is 0.1mm & 0.05mm. The 0.05mm diameter particles' diameter setup can be seen down below in Figure 3.24:

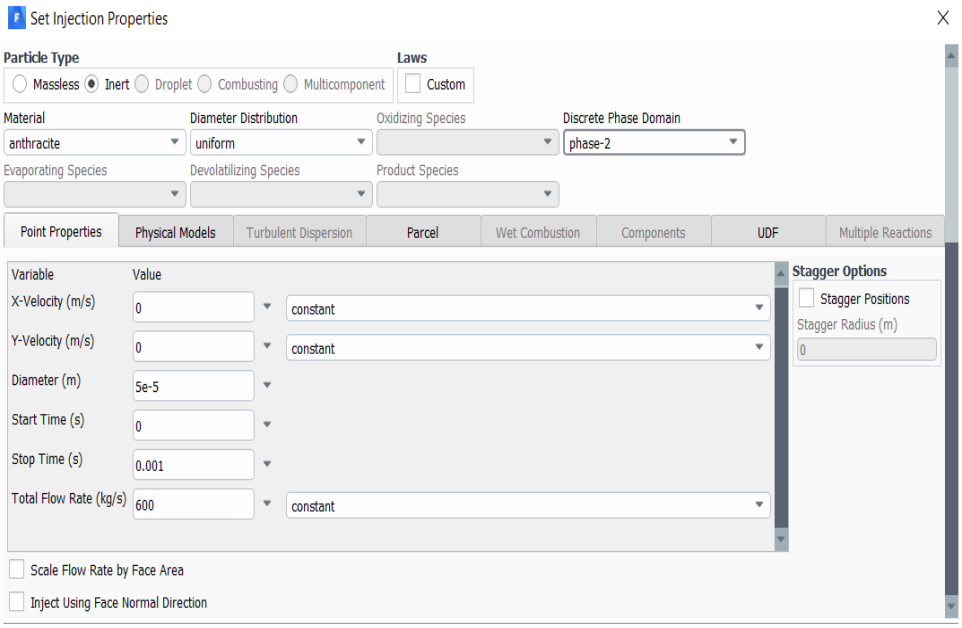

Figure 3.24: Defining 0.05mm diameter Particles, DDPM

To obtain an interface between pure water and particles the midline on geometry has been drawn like the previous chapter's Figure 3.10.

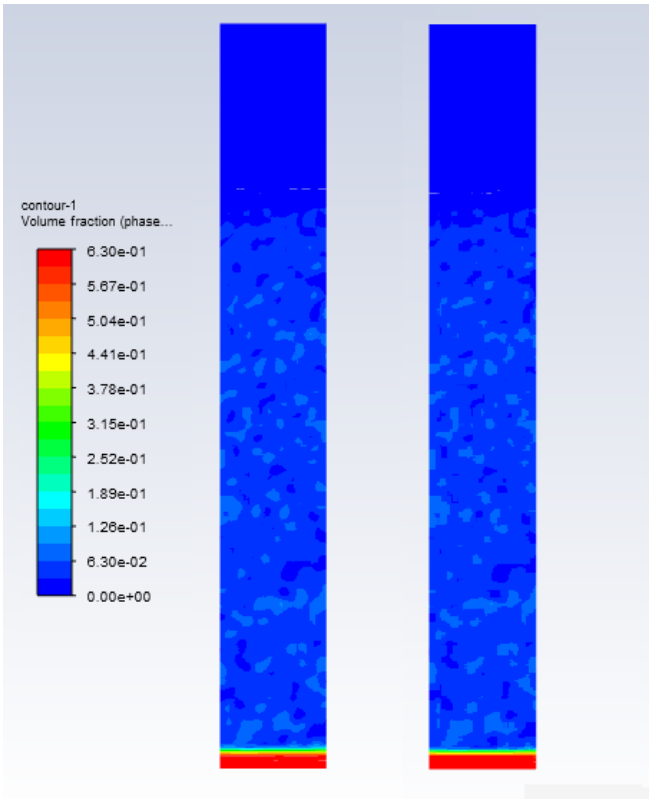

Figure 3.25: DDPM KTGF model, 0.1mm 5s (left) vs 0.05mm 20s (right)

Figure 3.25 illustrates the volume fraction contour which has been obtained for the particles' after the analysis. Contour results are similar to each other which can be seen in the figures.

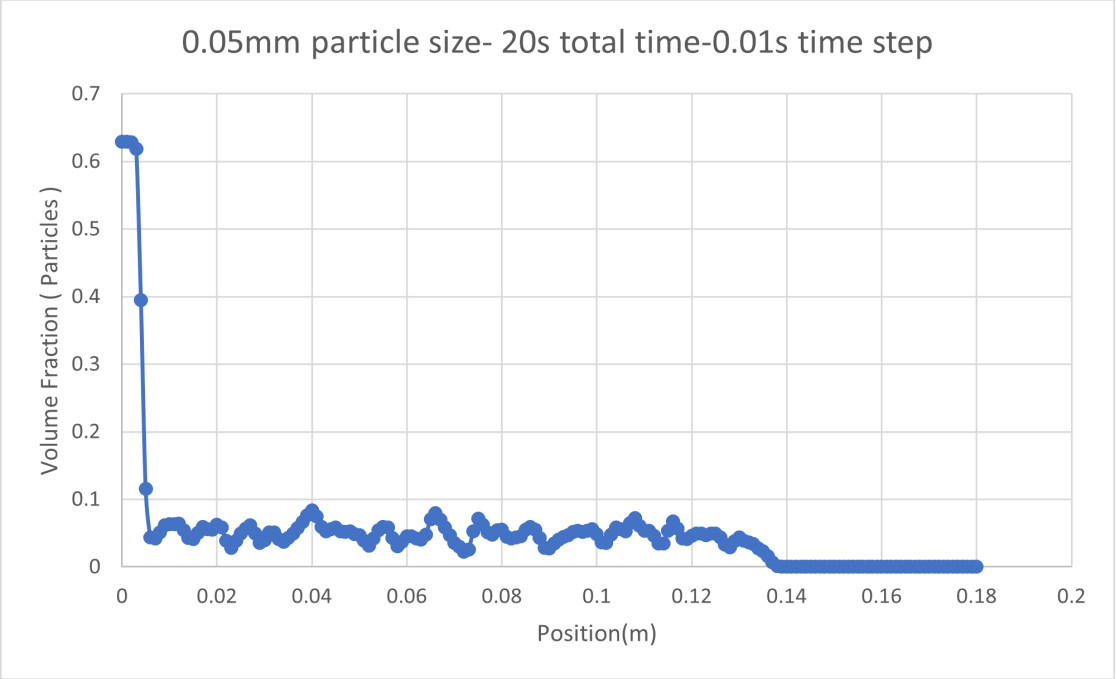

Figure 3.26: Volume fraction of the 0.05mm Particles according to Position

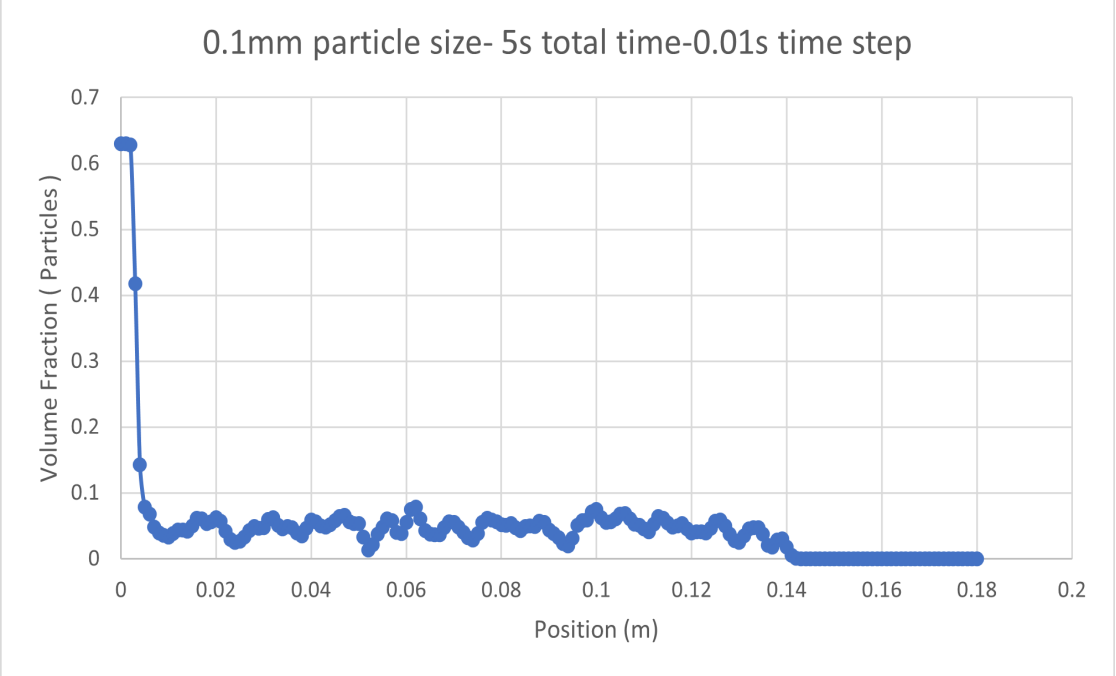

Figure 3.27: Volume fraction of the 0.1mm Particles according to Position

Figure 3.26 & Figure 3.27 show interface between pure water and particles for different particle sizes as in Figure 3.25 above. The interface height is similar to each other,which is approximately 0.14m.

As a result of the DDPM-KTGF method comparison for different sized particles, simulation with bigger particles does have practical meanings and it will be used for the following section.

3.3.2 2D and 3D models comparison

After making similarity analysis between different particle sizes of Euler and DDPM-KTGF models for 2D geometries, it's also necessary to compare the 2D geometry results of certain particle sizes with the 3D models.

The initial 3D model representing a water column which was created as a 180mm x 26mm diameter cylinder, and the generated mesh is depicted in Figure 3.28a

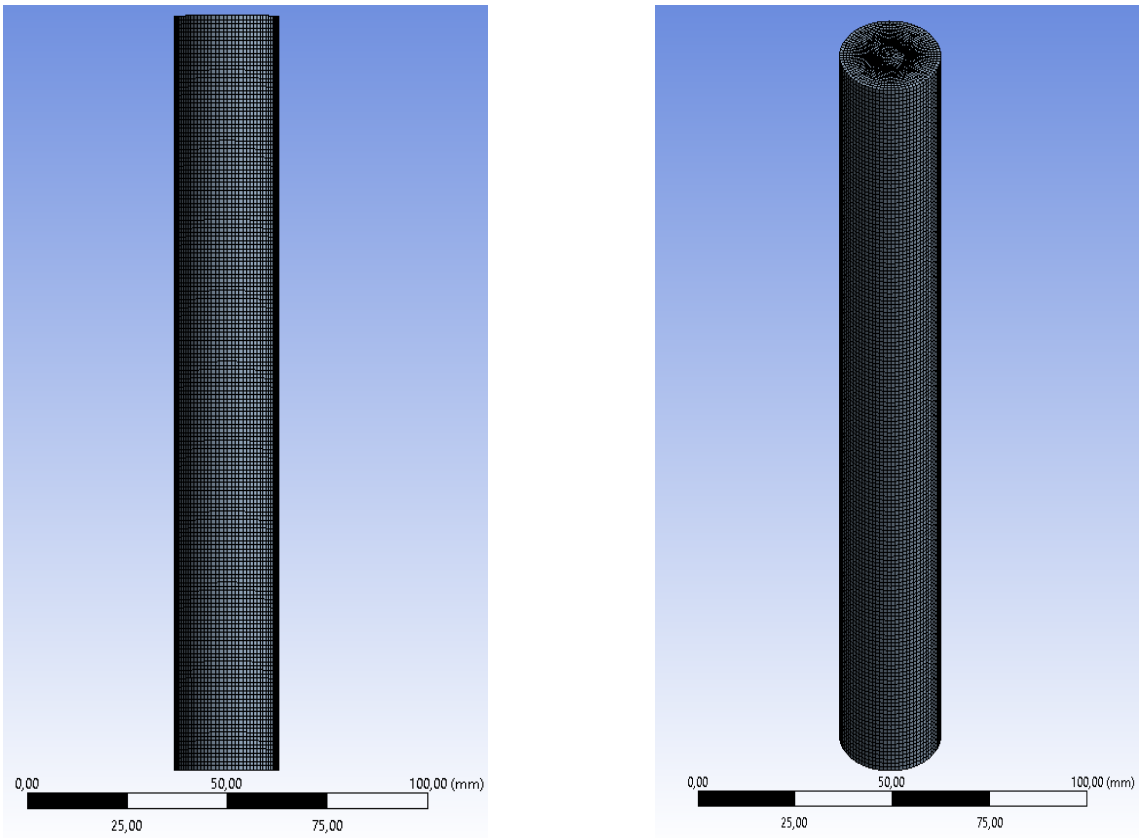

(a) 3D Model & Mesh-1 (b) 3D Model & Mesh-2

Figure 3.28: 3D Euler Mesh

During meshing, element size was defined as 1mm. Hence, the total number of nodes and elements as can be seen in Table 3.4:

Nodes	254240
Elements	246509

Table 3.4: Nodes & Elements

The mesh quality according to skewness and orthogonal quality as can be seen in Table 3.5:

	Min	Max	Average
Skewness	1.3057e-010	0.53217	8.2905e-002
Orthogonal Quality	0.49367	1	0.98758

Table 3.5: Mesh Quality

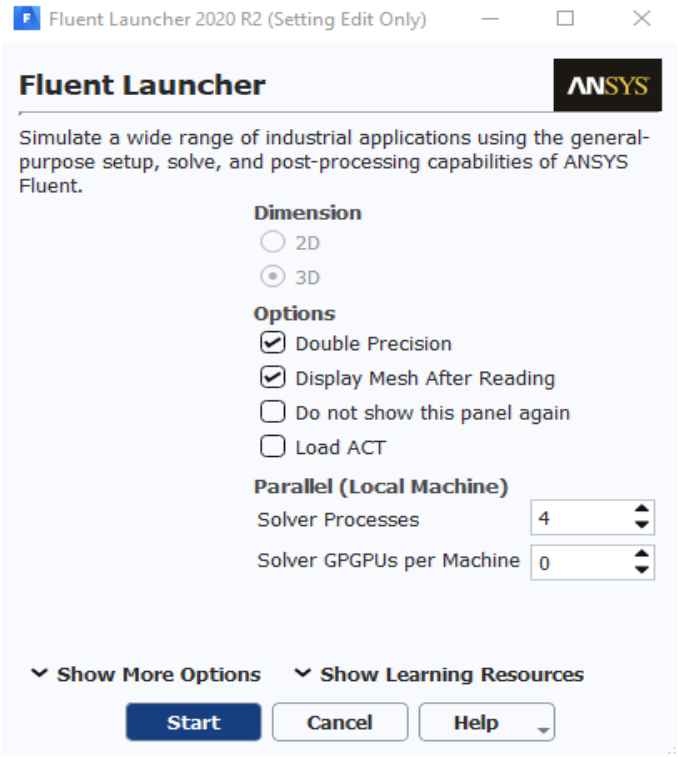

Figure 3.29: Fluent Launcher Setup - 3D Model

The same setup has been used for 3D analysis just like the 2D Model setup, the dimension is changed to 3D from 2D as can be seen in Figure 3.29. The 3D analysis for The Euler model has taken 5 hours in total with the system had described before. The volume fraction contour of the 3D model can be seen in the Figure 3.30a:

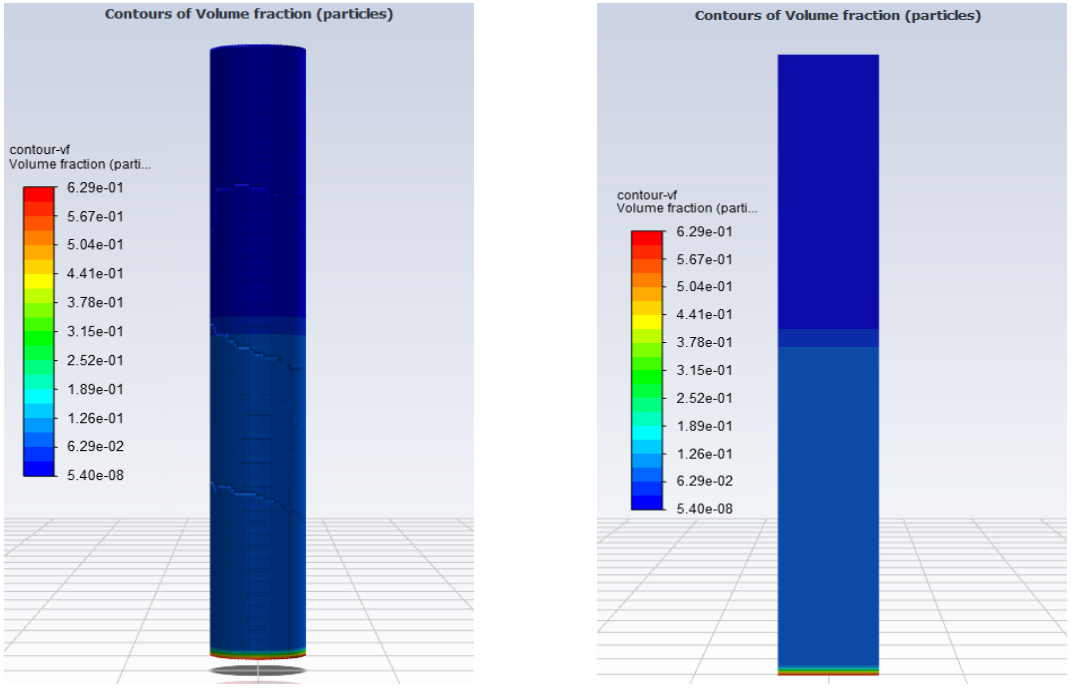

(a) 3D Contour (b) cross-section

Figure 3.30: 3D Euler Contour

After creating a plane of the cross-section of the cylinder geometry from the X-Y plane, the volume fraction contour can be seen in Figure 3.30b:

A line is created in the middle of the 3D geometry with the starting point of [0,0,0] and the ending point of [0,0.18,0], to obtain data of the interface between pure water and particles, as seen in Figure 3.31;

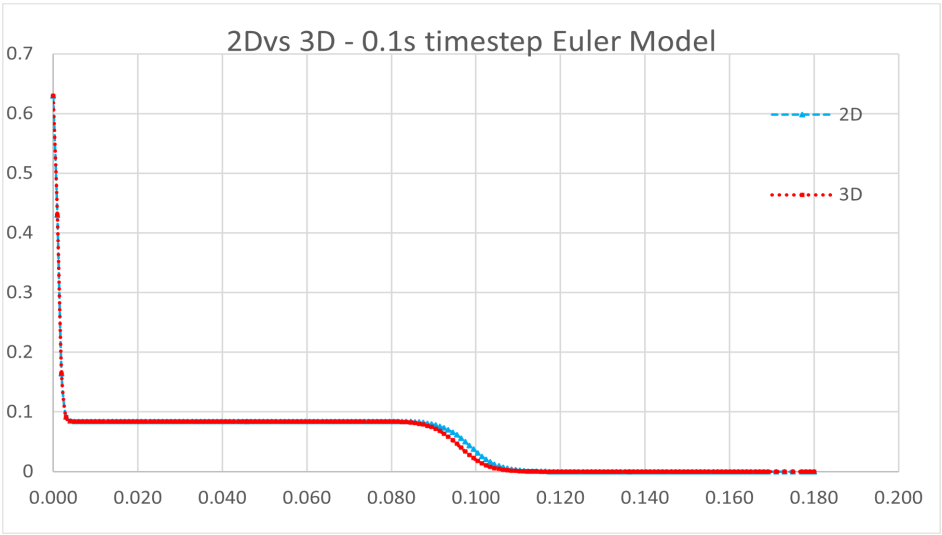

Figure 3.31: 2D vs 3D Euler Model 0.1mm particle size - 12.18s total time

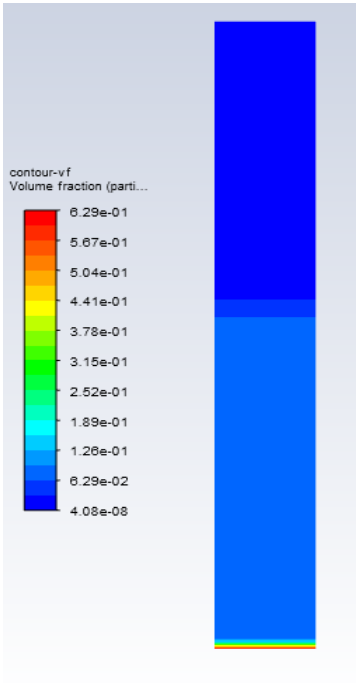

Figure 3.32: 2D Euler Model 0.1mm particle size - 12.18s total time

Figure 3.30b and 3.32 show the fraction contour, Figure 3.31 interface between pure water and particles obtained from 2D model. The interface height is similar to the value we obtained from the 3D model, which is approximately 0.12m. It means that 2D geometry is sufficient enough to obtain analysis data in this situation. As a result of the comparison of the 2D and 3D models, 2D model is sufficient and more time-efficient, thus it will be used for the following sections.

After comparing 2D and 3D Euler models, the same comparison is continued with the DDPM model. The fluent launcher had been set with same options with 3D Euler model. The DDPM model's 3D geometry is also shown in Figure 3.28a, the setup of the DDPM model has the same with the previous DDPM model setups and the total time has been set to 12.18s. The 3D analysis for DDPM model has taken 54 hours in total with the system had described before.

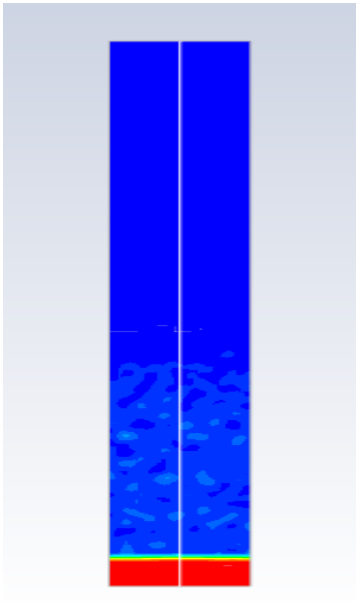

Figure 3.33: DDPM Geometry midline

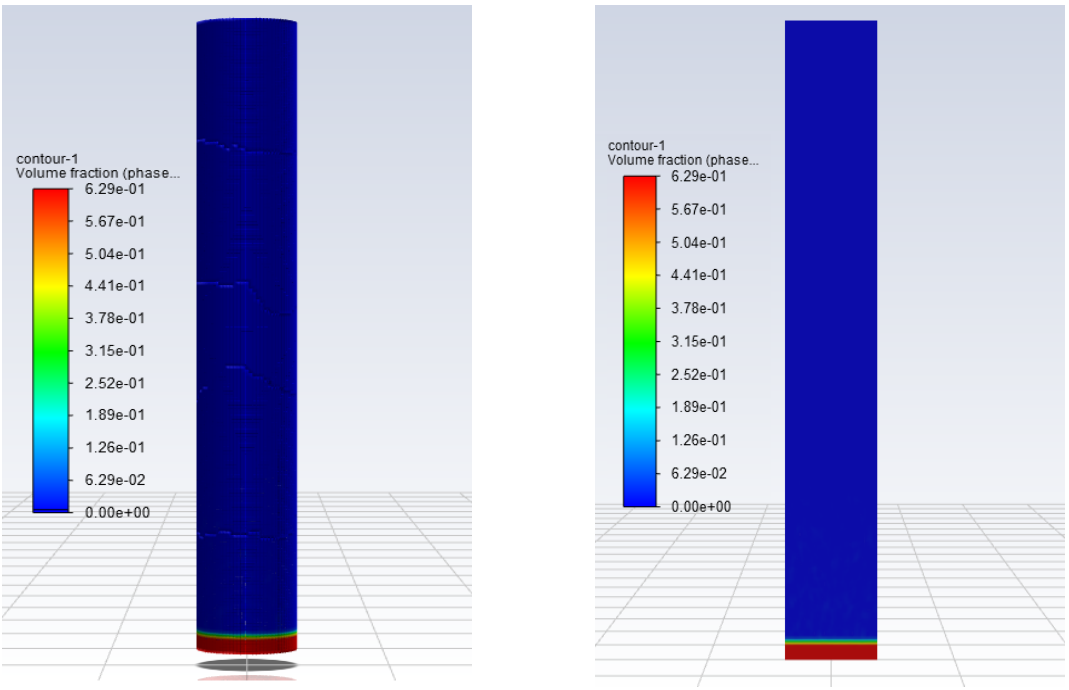

(a) 3D Contour (b) cross-section

Figure 3.34: 3D DDPM Model

To observe interface between pure water and particles for 3D model. Maximum packing limit reduced to 0.005 for the plane contour.

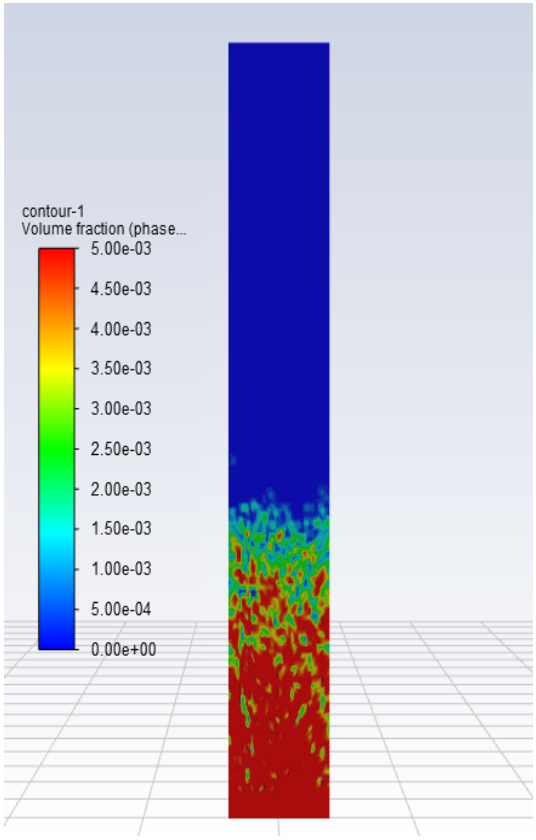

Figure 3.35: 3D DDPM Model - Reduced Max. Packing Limit

The 2D DDPM model's volume fraction contour for different time steps can be seen in Figure 3.36.

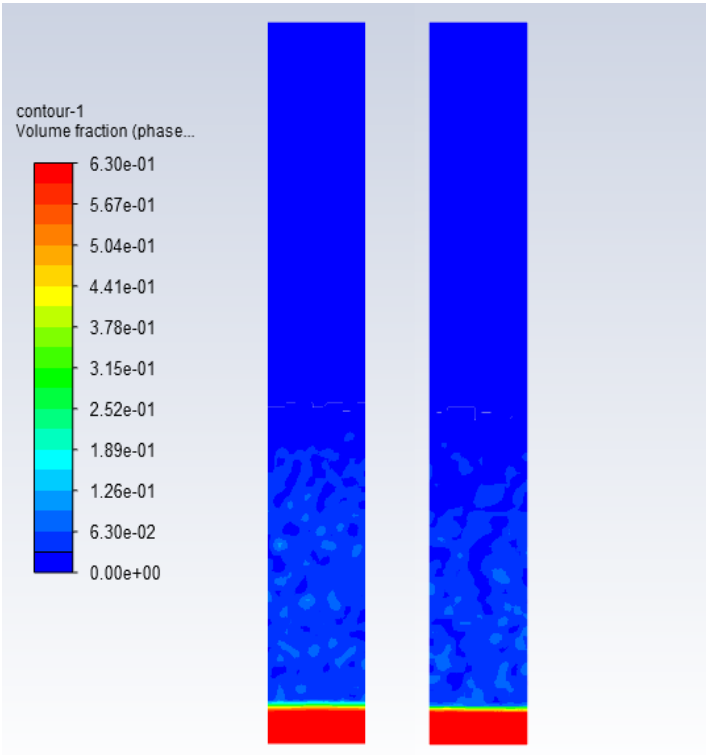

Figure 3.36: 2D DDPM Model - 0.01s time step (left) vs 0.003s time step (right) for 12.18s

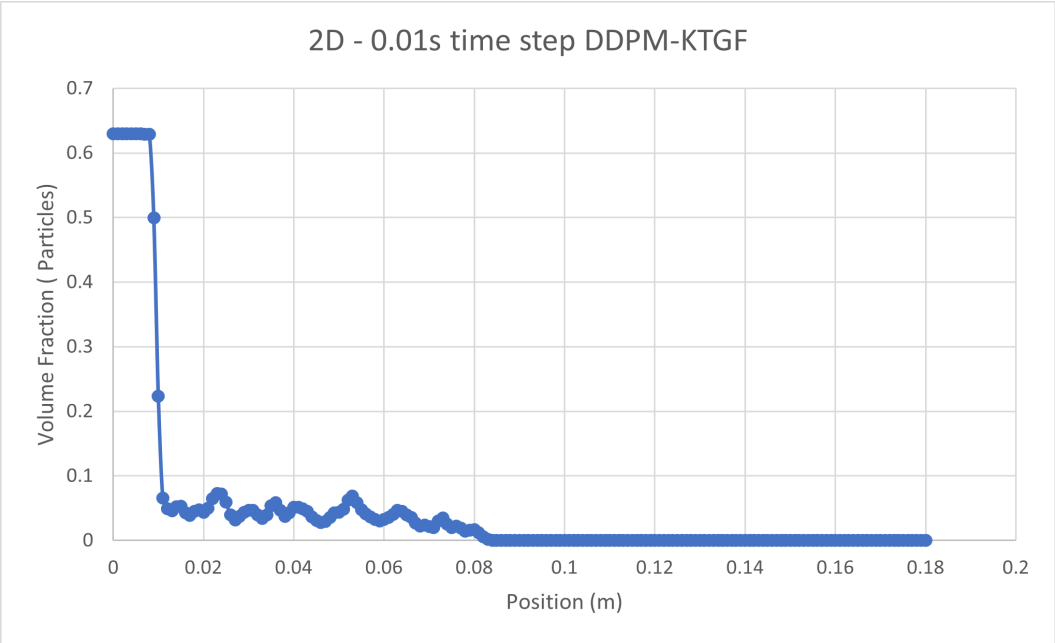

Figure 3.37: DDPM Model 0.1mm particle size- 0.01s time step - 12.18s total time

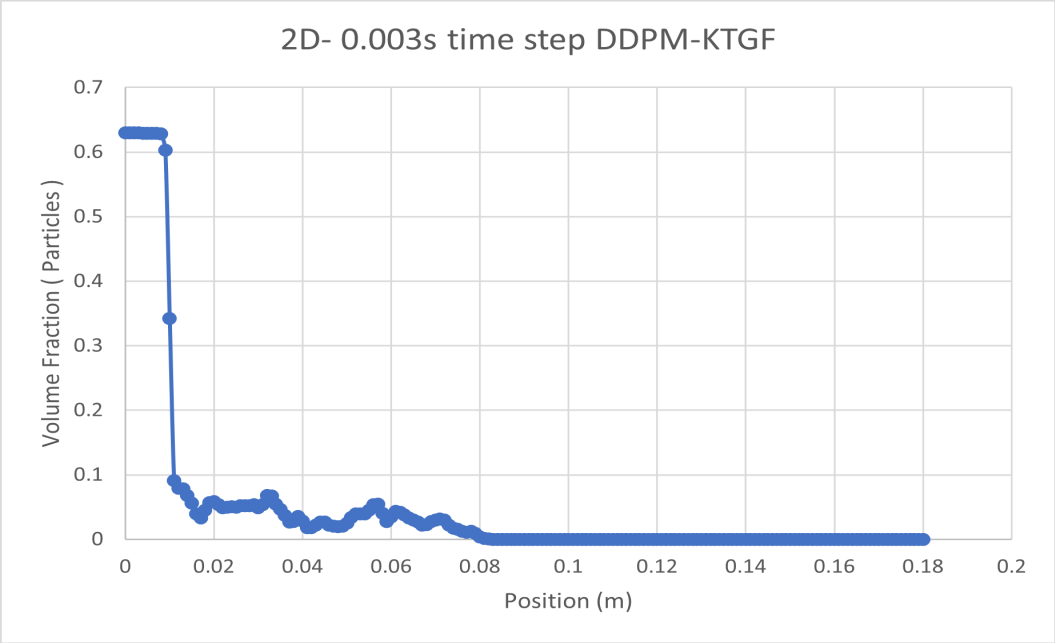

Figure 3.38: DDPM Model 0.1mm particle size- 0.03s time step - 12.18s total time

Figure 3.35 and 3.36 show the fraction contour of 3D & and 2D geometry. Figure 3.37 and 3.38 show the interface between pure water and particles obtained from the 2D model with different time steps. The interface height is similar to the value we obtained from the 3D model, which is approximately 0.08m. It means that 2D geometry is sufficient enough to obtain analysis data in this situation. Also for bigger time steps such as 0.01s, similar results have been obtained. As a result of the comparison of the 2D and 3D models, 2D model is sufficient and more time-efficient, thus it will be used for the following sections.

3.3.3 Total time comparison regarding to the particle size vs real experiments

The analysis geometries had drawn according to real experiment scales. The water height in the real experiment is 180.62mm, so the geometries of models are also set as 180mm. In the visual of the real experiment, the red lines are expressing 163.5mm out of 180.62mm. For the distribution of the particle diameters, ultrasonic measurement had been done. The distribution can be seen down below in Figure 3.40 which shows containing percentage for specific diameter values of total particles. The arithmetic means diameter of the particles is 2.85 μm which is approximately 62%. It also has particles smaller than 2.85μm, so the estimated interface height is lower than the 163.5mm and around 100mm to 110mm according to distribution.

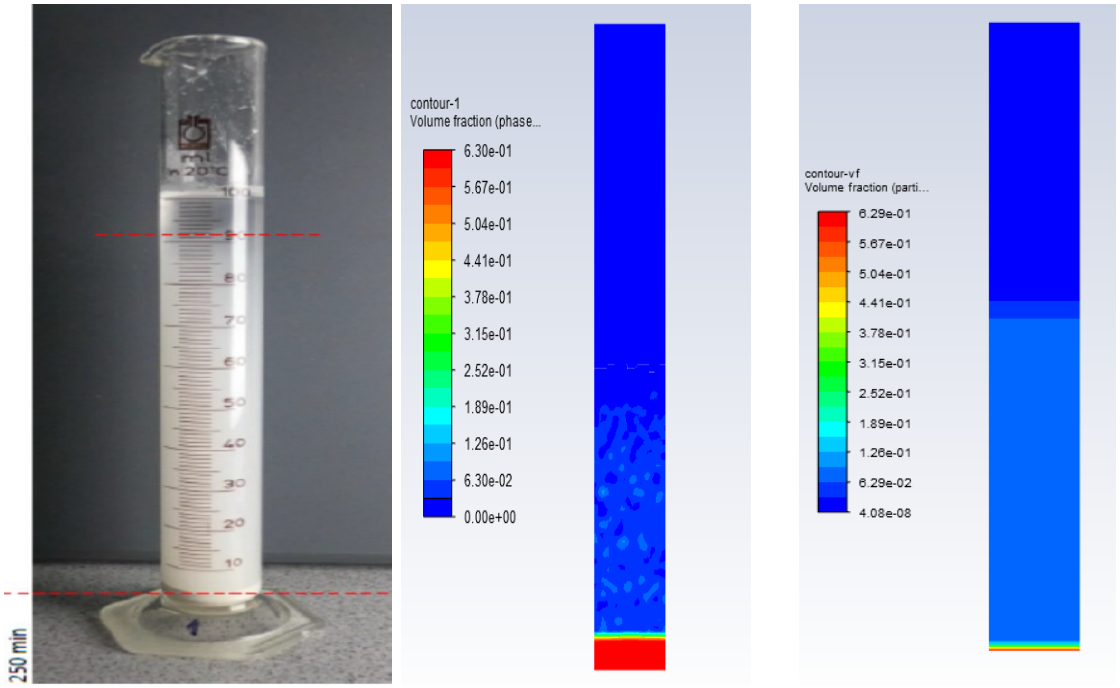

(a) Real Experiment Visual (b) 2D DDPM Model (c) 2D Euler Model

Figure 3.39: Comparison of Real Experiment & 2D DDPM & 2D Euler

According to the comparison of Euler & DDPM models from Figure **??** and Figure 3.37 with Real data, the Euler model is giving better results than DDPM. Thus, in the next chapter, the analysis will continue with the Euler model.

Meas.No. 4 | Date 11-26-2020 | Time 15:03 | Operator Moravec | ID 12118 | Serial No. 12118

Krida

Measuring Range	0.31 [µm] - 300.74 [µm]	Pump	100[rpm]
Resolution	62 Channels (17 mm / 114 mm)	Stirrer	3[rpm]
Absorption	9.00 [%]	Ultrasonic	100
Measurement Duration	3 [Scans]		

Modell Independant

Fraunhofer Calculation selected.

Interpolation Values... C:\Program Files\a22___32\fritsch\HIMNT_1.FPS

****** %	<=	0.050 µm	12.8 %	<=	1.000 µm	40.8 %	<=	2.000 µm
62.6 %	<=	3.000 µm	77.2 %	<=	4.000 µm	86.5 %	<=	5.000 µm
99.7 %	<=	10.000 µm	100.0 %	<=	20.000 µm	100.0 %	<=	50.000 µm
100.0 %	<=	100.000 µm	100.0 %	<=	200.000 µm	****** %	<=	300.000 µm

Interpolation Values... C:\Program Files\a22___32\fritsch\10_90.FPV

10.0 %	<=	0.897 µm	20.0 %	<=	1.253 µm	30.0 %	<=	1.601 µm
40.0 %	<=	1.968 µm	50.0 %	<=	2.378 µm	65.0 %	<=	3.139 µm
70.0 %	<=	3.453 µm	80.0 %	<=	4.249 µm	90.0 %	<=	5.535 µm
100.0 %	<=	11.438 µm						

Mean Values...

D43 =	2.85 µm	D42 =	2.26 µm	D41 =	1.77 µm	D40 =	1.4 µm
D32 =	1.78 µm	D31 =	1.39 µm	D30 =	1.11 µm		
D21 =	1.08 µm	D20 =	.87 µm				
D10 =	.9 µm						

Statistical Means...

Arithmetic Mean Diameter	2.854 µm	Variance	3.627 µm²
Geometric Mean Diameter	2.287 µm	Mean Squre Deviation	1.904 µm
Quadratic Square Mean Diameter	3.426 µm	Average Deviation	1.48 µm
Harmonic Mean Diameter	1.784 µm	Coefficiant of Variation	66.731 %

Statistical Modes...

Skewness	1.213	Mode	2.559 µm
Curtosis	1.395	Median	2.376 µm
Span	1.947	Mean/Median Ratio	1.201
Uniformity	.6		

Specific Surface Area	33630.21 cm²/cm³
Density	1. g/cc
Form Factor	1. g/cc

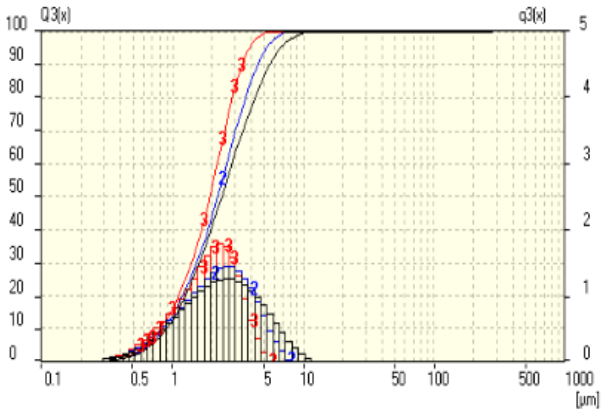

Figure 3.40: Particle characteristics measured by Dr. Moravec

3.4 Summary

In conclusion, the results in this chapter indicates that The Euler model can give us the same results for larger time steps therefore, we can save much more computational time and it is less computational demanding than DDPM. In the DDPM method, it's necessary to use smaller time steps, approximately 10 times smaller than the Euler method used during the analyses in this chapter, otherwise the incomplete particle tracking error occurs after a time.

For the time step analysis (GCI), as we can see it's hard to adapt that method to the DDPM-KTGF model because of the non-continuous phase of the model and it's hard to obtain balanced data from the slope of sedimentation analysis. Therefore, the Eulerian-Granular model is the better option for optimizing time steps rather than the DDPM-KTGF model for smaller particle analyses, which is highly time-consuming and computationally demanding.

It's necessary to make analyzes with simplified model geometries to find optimal time steps for specific sedimentation analysis. As a result of time step analysis of the Eulerian-Granular model error rate (%) increases while time step and total time are increasing but at the same time bigger time steps error ratio increasing ratio decreases and becomes closer to smaller time steps error ratio. Hence, the optimal time step for Eulerian-Granular model has been determined as 0.1 seconds.

To be able to use larger particles compared to real particles similarity analysis has been done as the last step. Analysis with the smaller particles with the size of micrometers can be highly computational demanding and analyzes can take several days. Also, it's a problem to have a sediment layer at the bottom and reach the packing limit, with the bigger time steps while trying to reduce necessary analysis time. After using Equation 3.32 and comparing the obtained results with real experimental data, Eulerian-Granular model has been decided to use for further analysis.

Chapter 4

Second model/ method

4.1 Lamella Clarifier

Lamella clarifier is a commonly used settler to remove particulates from liquids. In a lamella clarifier usually, a set of inclined plates are applied, these inclined plates can provide a large effective settling area for a small footprint, which improves the operating conditions of the clarifiers.

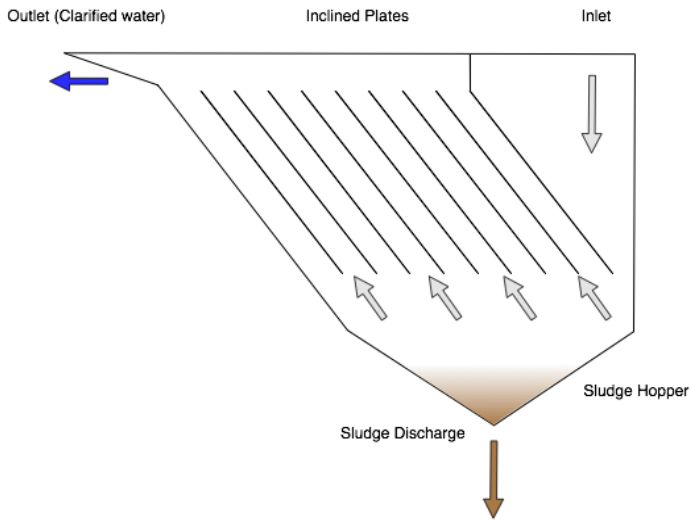

Figure 4.1: Lamella clarifier[16]

Figure 4.1 illustrates the working principle of a lamella clarifier. The inlet stream is stilled upon entry into the clarifier. Solid particles begin to settle on the inclined plates and begin to accumulate in collection hoppers at the bottom of the clarifier unit. The sludge is drawn off at the bottom of the hoppers and the clarified liquid exits the unit at the top over a weir[17].

The main feature, as well as the advantage of lamella clarifiers, is the usage of inclined plated, which is much more compact, usually requiring only 65-80 % of the area of clarifiers operating without inclined plates[18]. Therefore, a lamella clarifier is a better option when site footprint is limited. Furthermore, the small required space of lamella clarifier makes it possible to be set at indoor area, this possibility in return makes it easier to control temperature and pressure conditions, it can also avoid problems like algae growth, clogging due to blowing debris accumulation and odour control[19]. The inclined plates mean the clarifier can operate with overflow rates 2 to 4 times that of traditional clarifiers which allow a greater influent flow rate and thus a more time efficient clarification process[19]. However, Lamella clarifiers are not applicable for most raw feed mixtures. For these mixtures, pre-treatment is needed to remove materials that could drag down the separation efficiency.

Lamella clarifier is typically used at field such as fly ash waste, flue gas desulfurization waste, clarification, iron removal, heavy metals removal, filter press belt wash. battery plant heavy metals removal, hazardous waste remediation, and so on.

4.2 Geometry of the model

The geometry of the second model is based on the real geometry which had been used in the real experiment in Czech Technical University laboratories.

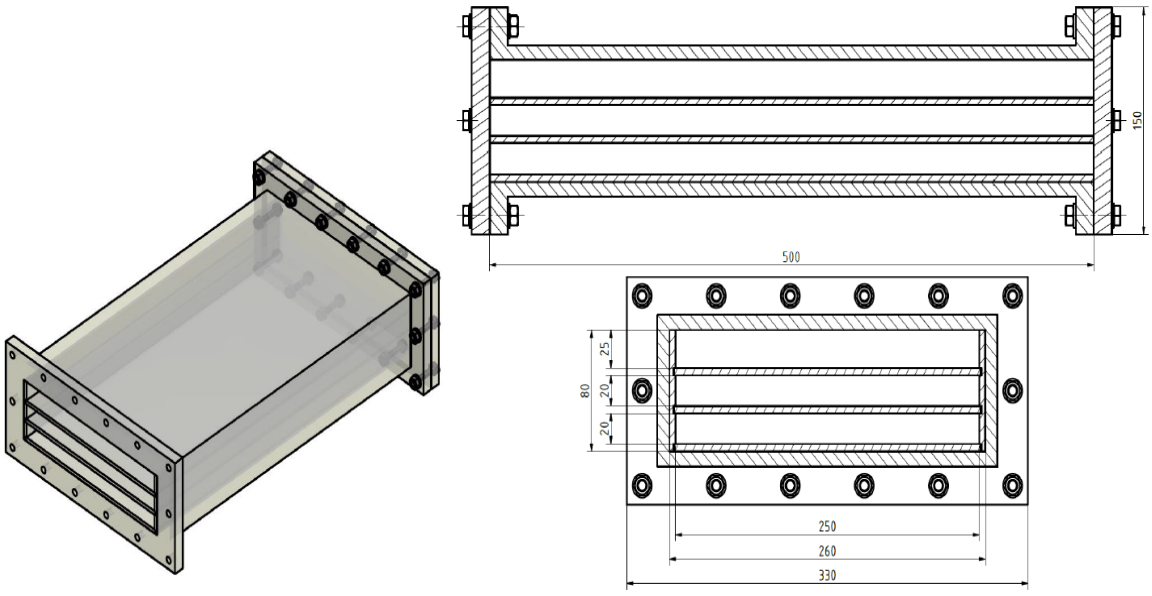

Figure 4.2: Real Lamella Model geometry

The ANSYS model has same geometry of middle lamella separator, which is a 20mm x 500mm rectangle as seen in Figure 4.2. The left side of the geometry was divided

into two edges, one of 16 mm length as the inlet, and the second edge of 4 mm below was set as the outlet for particles, as seen in Figure 4.3.

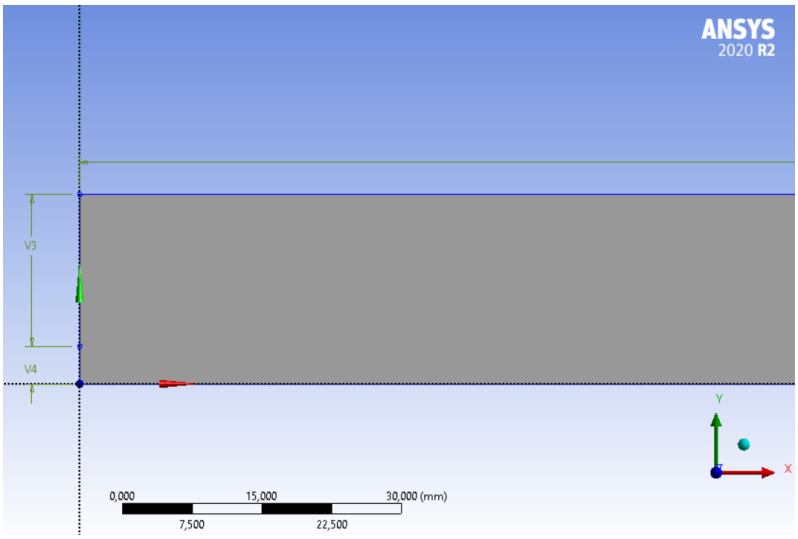

Figure 4.3: Lamella Model geometry

During meshing, element size was defined as 1mm, it can be seen in Figure 4.4. Hence, the total number of nodes and elements are shown in Table 4.1:

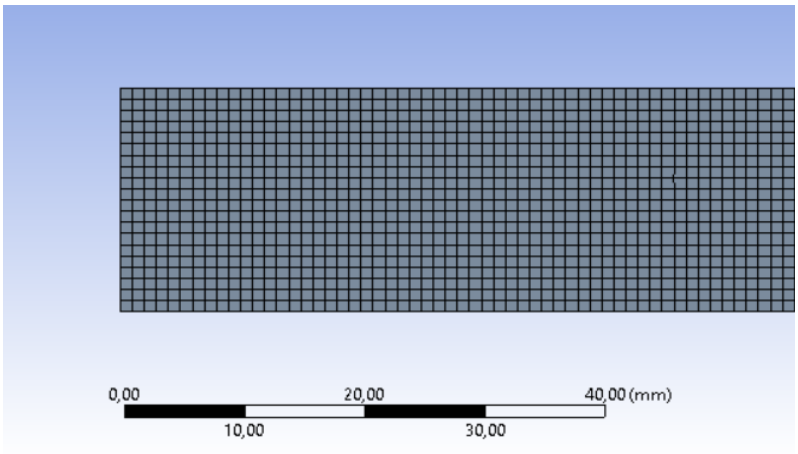

Figure 4.4: Mesh Element Size

Nodes	10521
Elements	10000

Table 4.1: Nodes & Elements

The mesh quality for a simple rectangular geometry is close to perfect. It means that skewness is close to 0 and orthogonal quality is close to 1.

After meshing, named selections had been created. A as inlet, B as outlet2 , C as outlet and D as wall which is the bottom and the top of the rectangular geometry. The named selections can be seen down below in Figure 4.5.

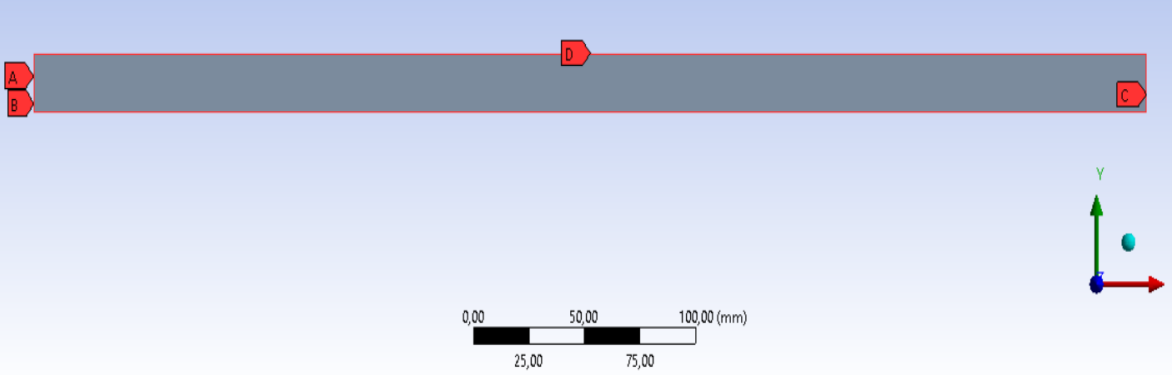

Figure 4.5: Named Selections A-B-C-D

After creating the mesh of the lamella geometry to obtain 15-30-45 degree, in domain tab, Transform -> Rotate... option had been used to rotate the geometries as can be seen in Figure 4.6, the geometries had obtained down below in Figure 4.7.

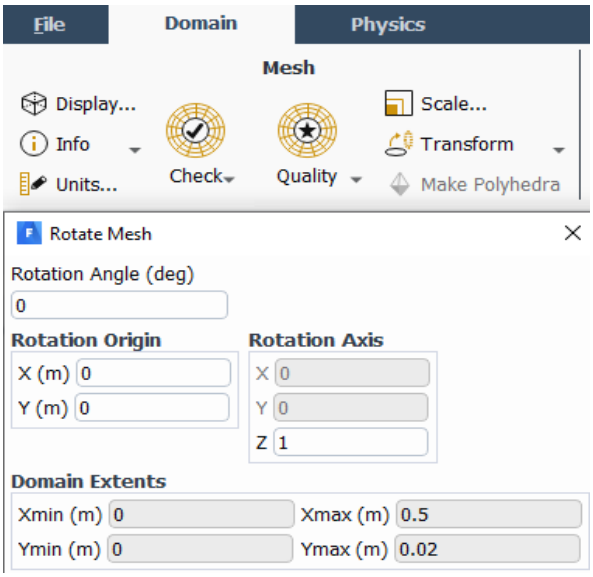

Figure 4.6: Rotating the Mesh

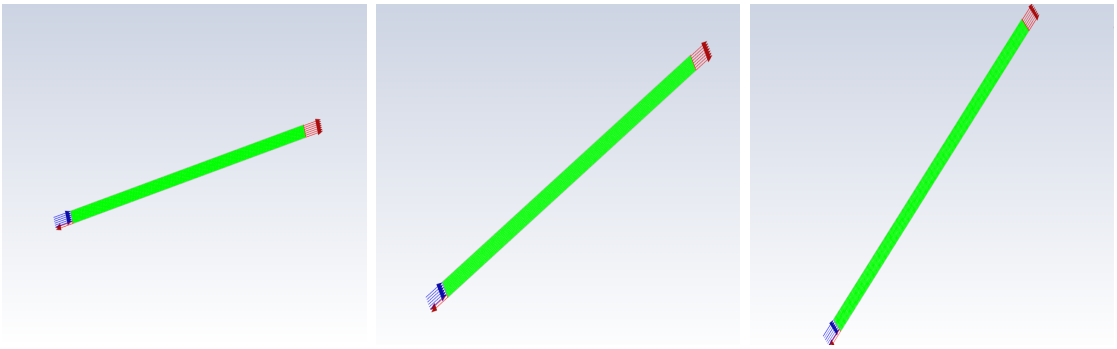

(a) 15 degree (b) 30 degree (c) 45 degree

Figure 4.7: Visual of Geometries

4.3 CFD setup for chosen model

After running set of analyses for 0.1 mm diameter particles, the data have obtained wasn't enough to comparison the results. Therefore, particle diameter reduced to 0.01mm. For the geometries, velocity magnitude between 0.01-0.2 [m/s] had been used for particles with 0.01 mm diameter. Before starting the setup the model, the Reynolds number must be calculated for chosen velocity magnitudes to determine turbulent and laminar flow.

The Reynolds number is defined as the ratio between the inertial forces and the viscous forces of a fluid undergoing an internal movement caused by the different velocities of the fluid, and it is a guide to determine whether the turbulent flow occurs in a situation. The region where these forces change their behaviour is called the boundary layer. A comparable effect can be generated by introducing a high-velocity flow into a low-velocity fluid. This generates fluid friction, which develops turbulent flow. The factor that tends to counter this effect is the fluid's viscosity, which tries to inhibit turbulence.

For this analysis it's necessary to calculate Reynolds number for internal flows. Reynolds number range for laminar regime is up to 2300, for transient regime 2300>Re>4000 and for turbulent regime Re>4000. During the laminar regime, the viscous forces are the dominant ones, the movement of the fluid is regular and constant in a close channel. During the turbulent, regime is dominated by inertial forces that produce flow instabilities and vortexes.

The formula to calculate the number of Reynolds is:

$$Re = \frac{\rho_{fluid} u_{fluid} L_{characteristic}}{\mu_{fluid}} \tag{4.1}$$

Where ρ is the density of the fluid equal to 998.2 [kg/m^3] , u is the velocity magnitude between 0.01 to 0.2 [m/s], L is a characteristic linear dimension equal to 20 mm, and μ is the dynamic viscosity of the fluid equal to 0.001003[kg/ms] .

For the chosen 0.2 [m/s] velocity magnitude, the maximum value of Reynolds number is 3987 and for Re=2300, laminar and transient regime velocity magnitude is close to 0.125 [m/s]. Hence, velocity magnitudes had been chosen as 0.2-0.125-0.1-0.075-0.05-0.01 [m/s] for the first set of analyses.

Terminal velocity cannot be calculated directly because the region of settling is unknown. In this case, the region is determined by the value of Reynolds number which contains unknown terminal velocity u.

$$C_{Dt}Re^2 = \frac{4}{3}\frac{D(\rho_p - \rho_f)g}{u^2\rho_f}\frac{u^2D^2\rho_f^2}{\mu^2} = \frac{4}{3}\frac{D^3(\rho_p - \rho_f)\rho_f g}{\mu^2} \tag{4.2}$$

For Stokes region $C_{Dt}Re^2 < 48$:

$$u = \frac{D^2(\rho_p - \rho_f)g}{18\mu} \tag{4.3}$$

For Transition region $48 < C_{Dt}Re^2 < 1.1 \times 10^5$:

$$u = 0.153\frac{D^{1.14}(\rho_p - \rho_f)^{0.71}g^{0.71}}{\rho_f^{0.29}\mu^{0.43}} \tag{4.4}$$

For Newton region $1.1 \times 10^5 < C_{Dt}Re^2 < 4 \times 10^5$

$$u = 1.74\sqrt{\frac{D(\rho_p - \rho_f)g}{\rho}} \tag{4.5}$$

The terminal velocity of 0.01mm particles has been calculated according to equations down below where ρ for particles equal to 2560 [kg/m^3] . After calculating Equation 4.2 where C_{Dt} is $\frac{24}{Re}$, the result is 0.0202 for the given values which determined as Stokes region, which can be seen down below and the terminal velocity calculated as 0.000084767 [m/s] from the Equation 4.3.

For the laminar regime, the Euler model setup is the same as in previous chapter.

For the turbulent regime, realizable $k - \epsilon$ model has chosen. Enhanced wall treatment had chosen for the near wall treatment. The rest options stayed default for the turbulent viscous model.

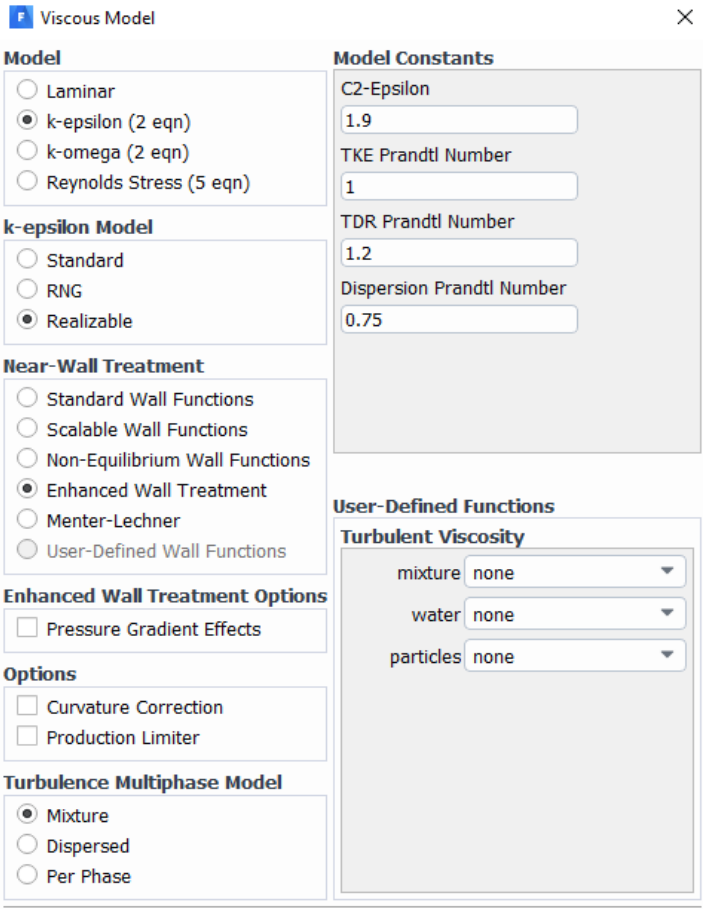

Figure 4.8: Turbulent Setup

4.3.1 Boundary Condition

After finishing the model setup, the boundary conditions has been set for laminar and turbulent regime separately.

The momentum options for the mixture phase has been set as default for both laminar and turbulent regime as can be seen in the Figure 4.9 and Figure 4.10. For the laminar regime, Supersonic/Initial Gauge Pressure is set as 0 pascal and for the turbulent regime, Supersonic/Initial Gauge Pressure is set as 0 pascal, Specification Method is set as Intensity and Viscosity Ratio, Turbulent Intensity as 5 % and Turbulent Viscosity Ratio as 10.

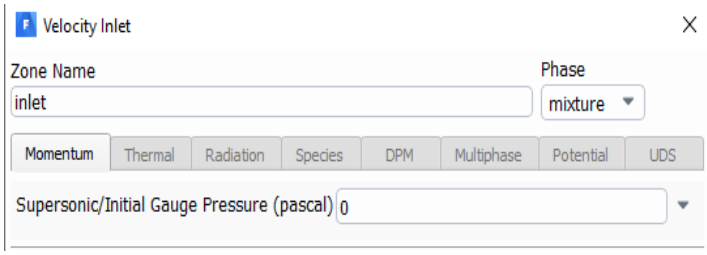

Figure 4.9: Boundary Condition Laminar Regime

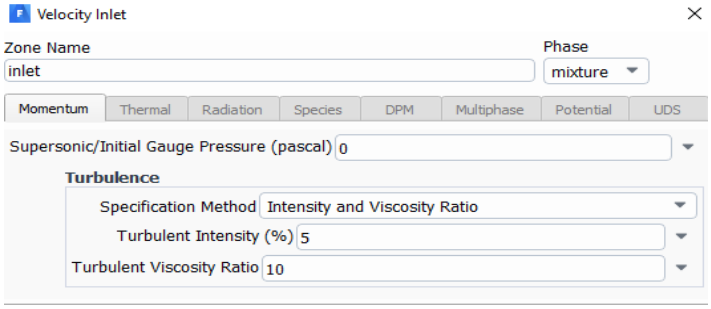

Figure 4.10: Boundary Condition Turbulent Regime

The particle and water phase has been set same for laminar and turbulent regime. An illustration of setup can be seen in Figure 4.11, Figure 4.12 and Figure 4.13. For the water phase, Velocity Specification Method is set as Magnitude, Normal to Boundary, Reference Frame is set as Absolute and Velocity Magnitude is set as mentioned values. For the particle phase, Velocity Specification Method is set as Magnitude, Normal to Boundary, Reference Frame is set as Absolute, Velocity Magnitude is set as mentioned values and Granular Temperature is set as 0.0001 [m^2/s^2].

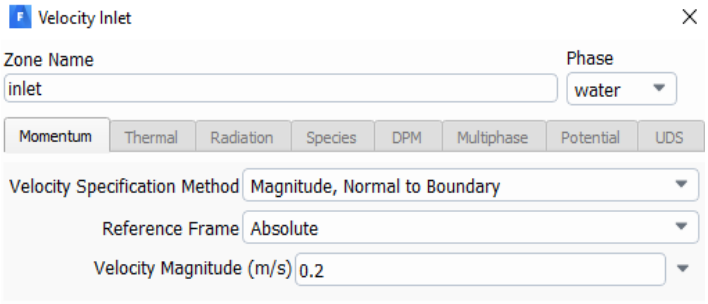

Figure 4.11: Boundary Condition Particle Setup

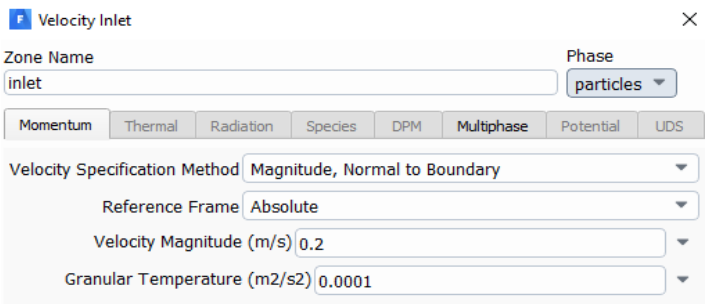

Figure 4.12: Boundary Condition Particle Setup-1

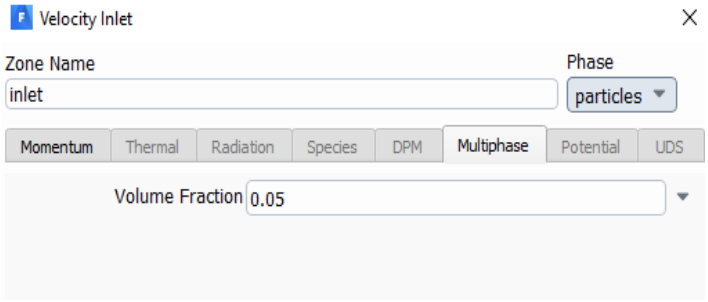

Figure 4.13: Boundary Condition Particle Setup-2

4.3.2 Report Definitions & Monitors

To track the leaving particles from the outlets during the analyses, report definitions & monitors had been defined for the inlet, outlet, outlet2.

For the inlet, outlet and outlet2, report definitions had been created for the mass flow rate of particles' phase for each boundary separately, to create monitors as the following step. The values are obtained from each average over (time steps) which can be seen in Figure 4.14. Same setup was done for outlet and outlet 2.

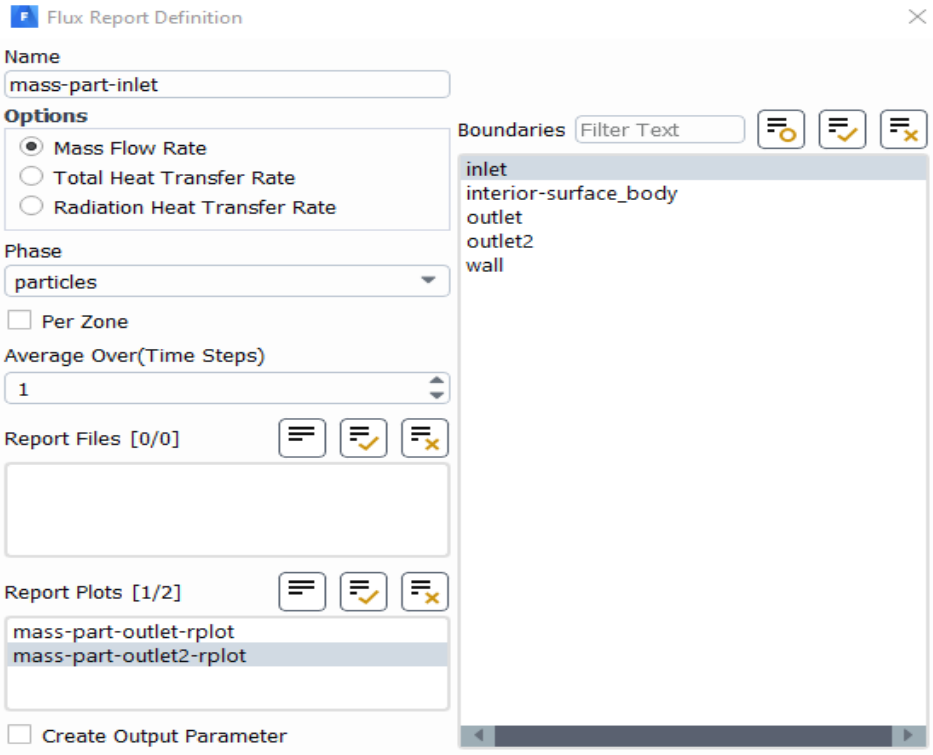

Figure 4.14: Report Definition for Inlet

The monitors have been created for particles' inlet and outlet to the lamella geometry. To create the monitors, the report definitions had been used. To track leaving particles from outlet, the mass-part-outlet has been added and data has obtained for every time

step where X-Axis represents the flow time and Y-Axis represents the mass flow rate, which can be seen in Figure 4.15. To track total values of particles for inlet and outlets, all available report definitions have been added and data has obtained for every time step where X-Axis represents the flow time and Y-Axis represents the mass flow rate, which can be seen in Figure 4.16.

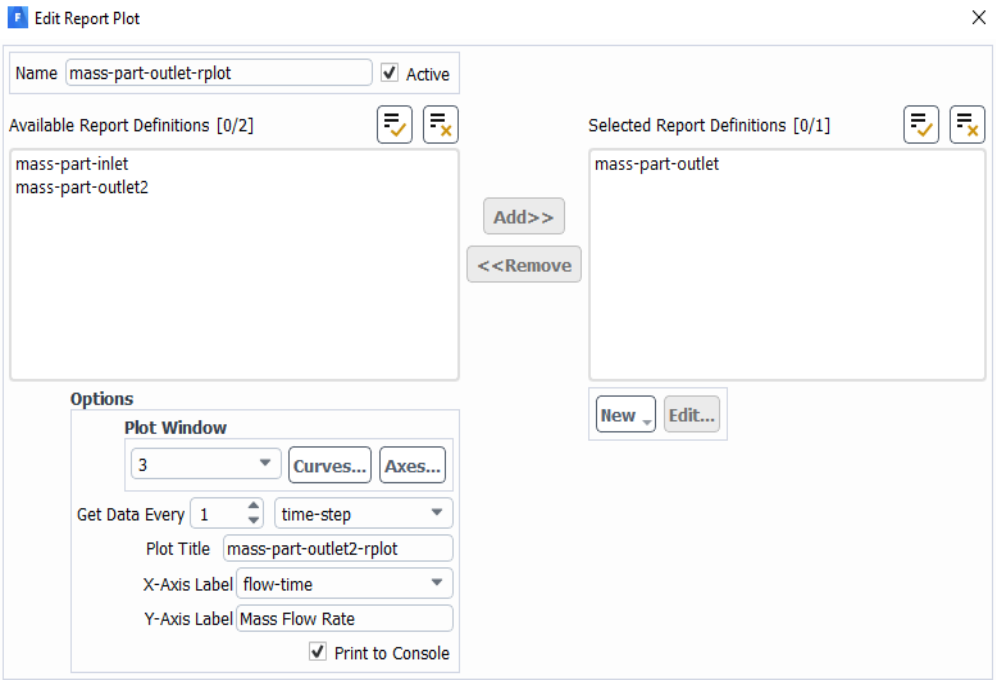

Figure 4.15: Monitor Plot Outlet

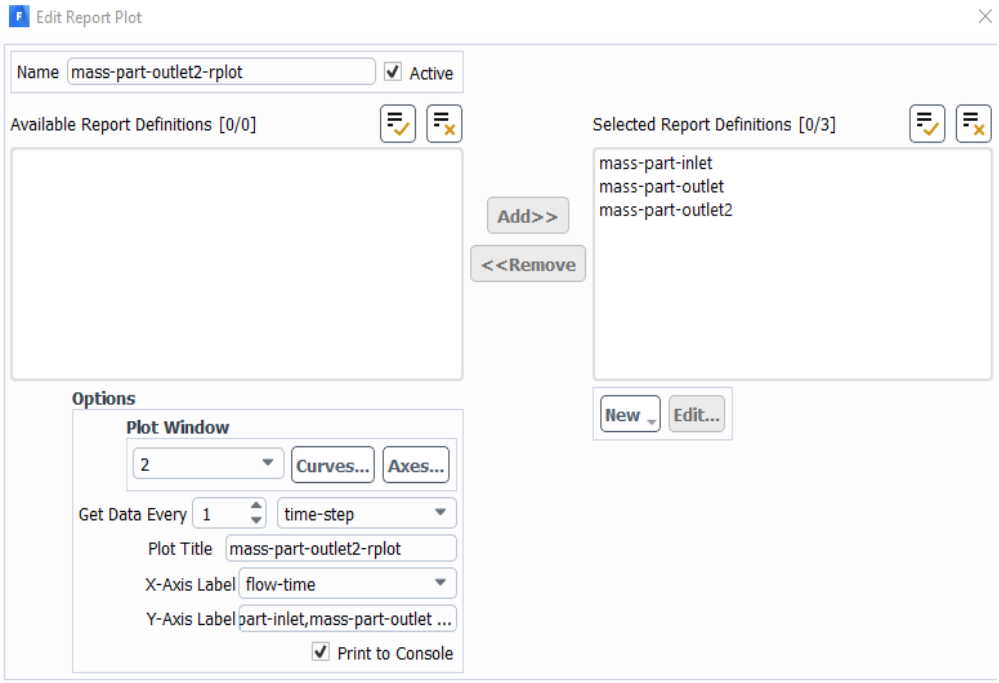

Figure 4.16: Monitor Plot Inlet-Outlet-Outlet 2

4.4 Results & Comparison

The post-processing results in ANSYS Fluent for transient simulations had been done for a 0.1s time step until the figure of the monitor plots reached a steady state. An example can be seen from the results in Figure 4.17 & Figure 4.18 where particles are leaving from the geometry.Hence, the mass flow rate has negative values. The analyses had been done for 15-30-45 degrees. The velocity magnitude of 0.01-0.05-0.075-0.1-0.125-0.2 [m/s] for 15 degrees and 0.05-0.075-0.1-0.125-0.2 [m/s] for 30-45 degrees had been used. The analyses had taken between 10 minutes to 23 hours for different angles and velocity magnitudes for the system mentioned earlier and total flow time changes between 25[s] to 8000 [s] .

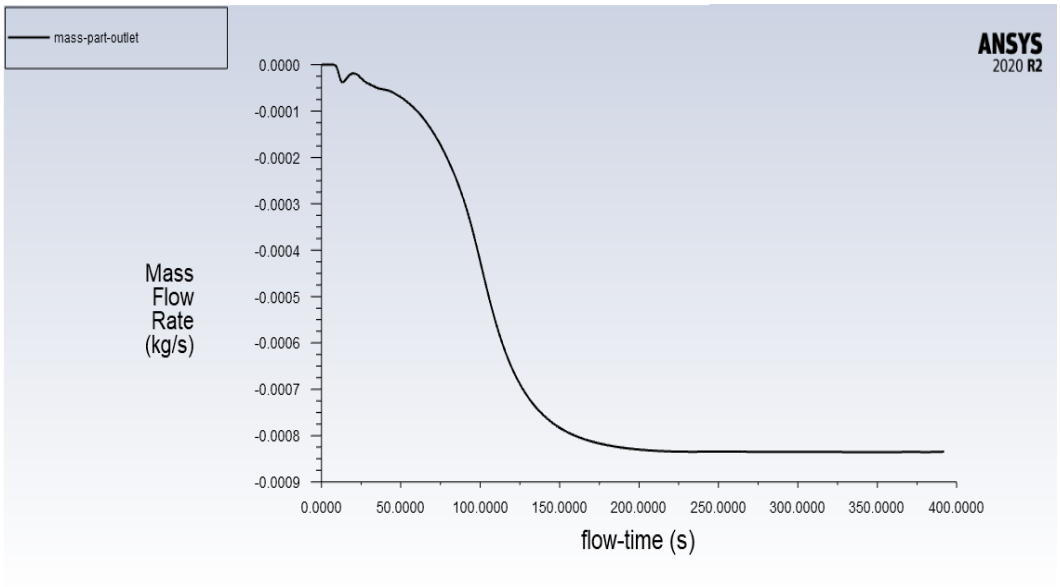

Figure 4.17: Example Monitor Plot Outlet

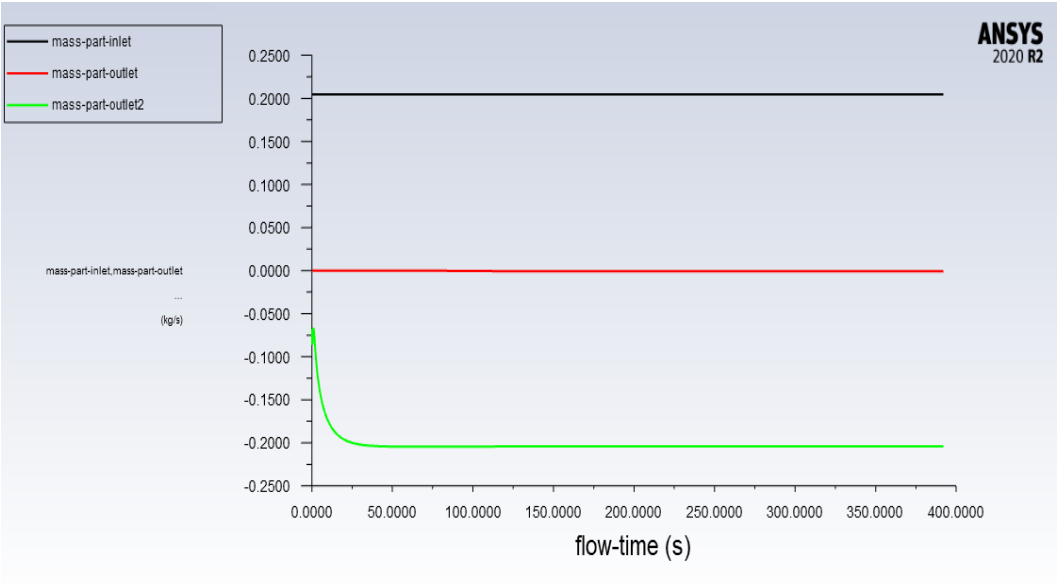

Figure 4.18: Example Monitor Plot Inlet-Outlet-Outlet 2

4.4.1 Effect of Velocity Magnitude

In this section, the effect of velocity magnitude on particles has been aimed to obtain. The change of the volume fraction for different velocity magnitudes and its effect on the sludge layer of the particles can be seen in Figure 4.19.

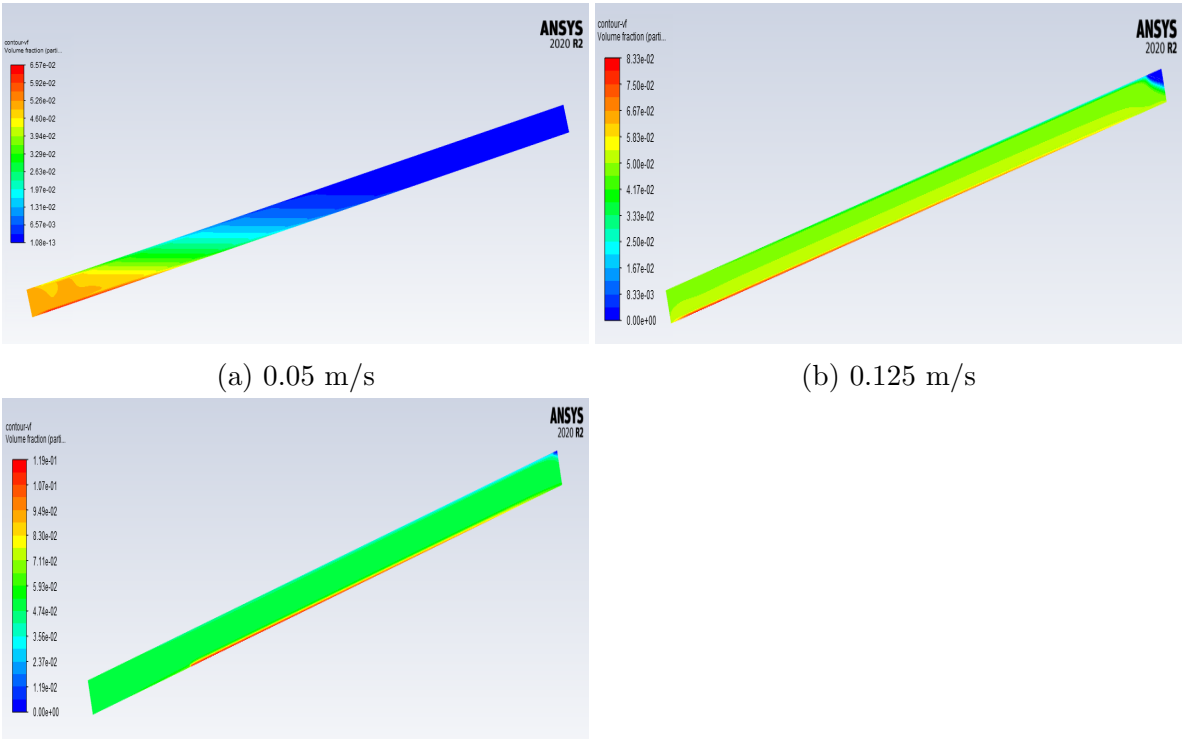

(a) 0.05 m/s

(b) 0.125 m/s

(c) 0.2 m/s

Figure 4.19: Example- Against the Velocity Magnitude for 15 degree

The higher velocity effect can be seen on the sludge layer of the particles. The higher velocity magnitude spreads the layer at the bottom of the clarifier and drags it to the top. The change of the values for each velocity magnitude for a specific angle can be seen in Figure 4.20. The particles are leaving from outlets, hence mass flow rate values are negative in the following Figure.

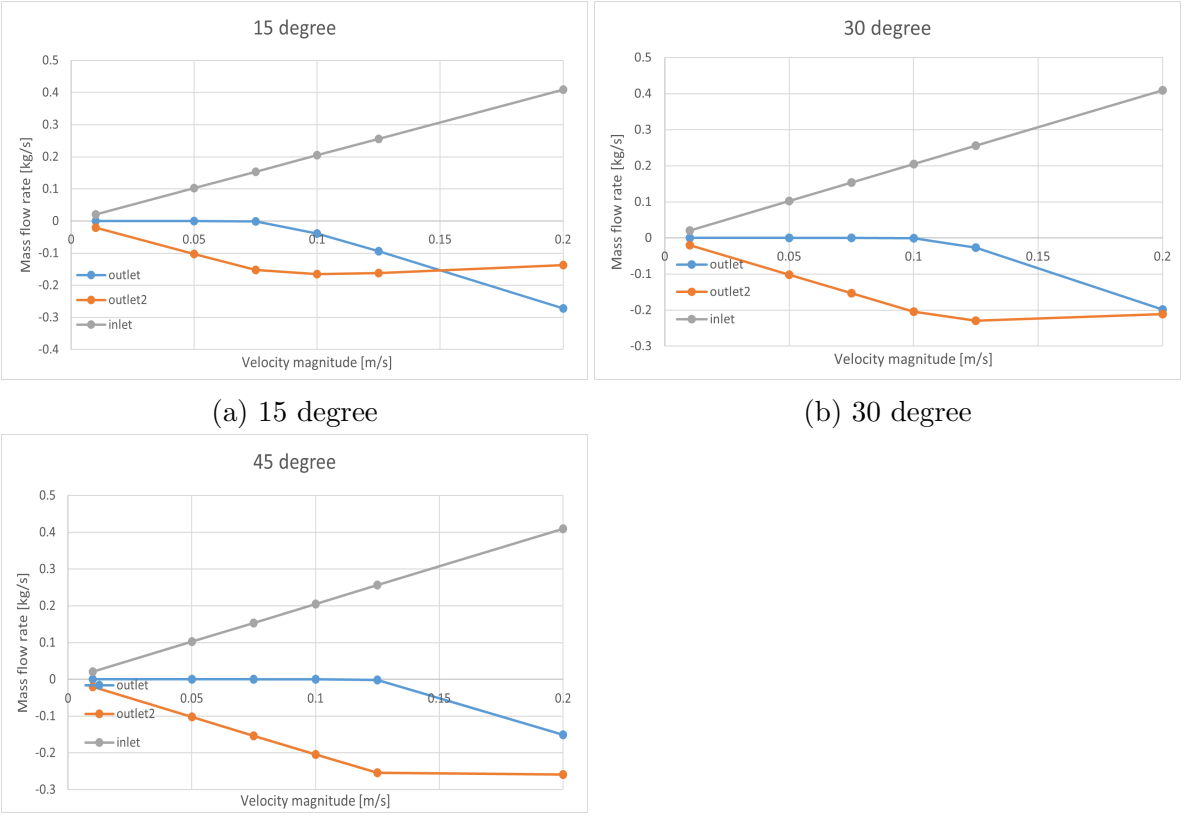

(a) 15 degree

(b) 30 degree

(c) 45 degree

Figure 4.20: Mass flow rate regarding velocity magnitude of water

It can be observed from Figure 4.20 that when the velocity magnitude increases total mass flow rate and mass flow of leaving particle increase. Also, the mass flow rate of leaving particles from the outlet increases and, outlet 2 decreases. According to the results, the sedimentation effectiveness is better for greater inclination angles.

4.4.2 Effect of Inclination angle

In this section, the effect of inclination angle on particles has been investigated. The change of the volume fraction for different inclination angles and its effect on the layer of the particles can be seen in Figure 4.21.

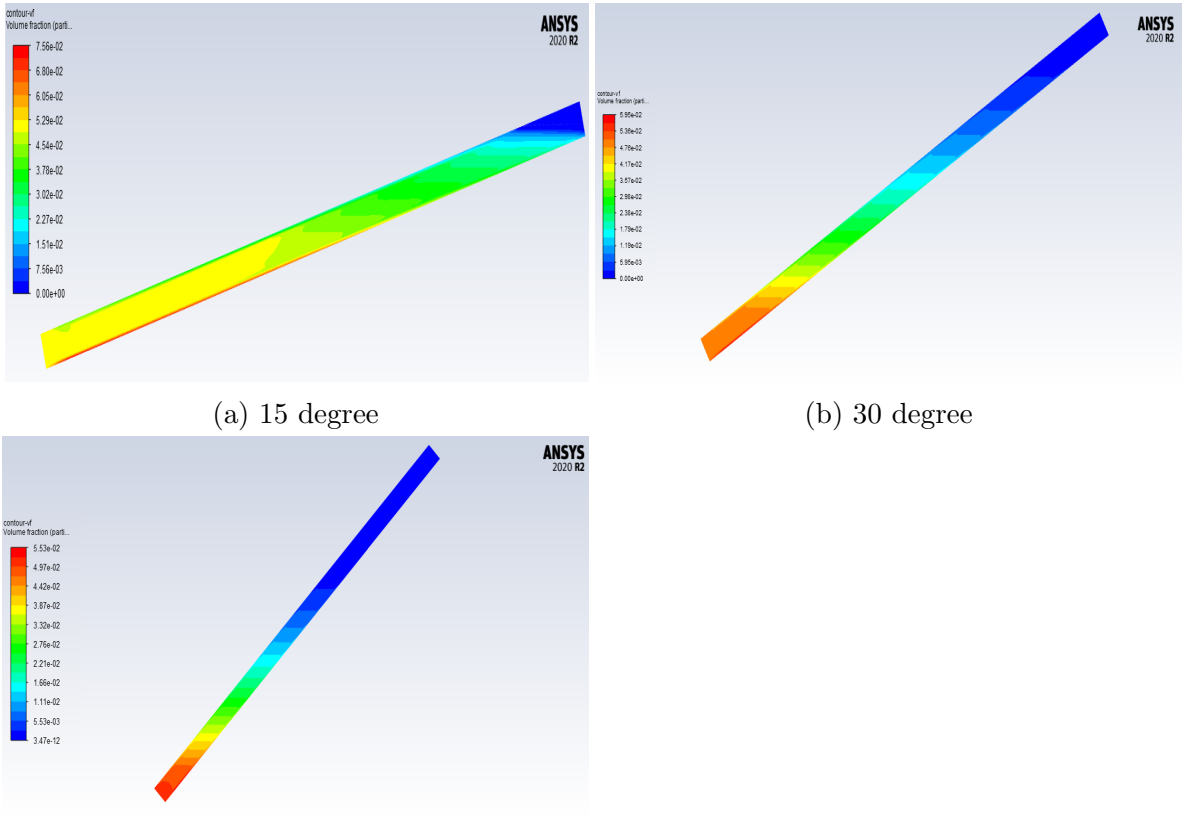

(a) 15 degree

(b) 30 degree

(c) 45 degree

Figure 4.21: Visual against the Inclination angle

The greater inclination angle effect can be seen on the layer of the particles. The greater inclination angle drags the layer of the particles to the bottom of the clarifier and reduces the amount of leaving particles from the outlet. The change of the values for each inclination angle for a specific velocity magnitude can be seen in Figure 4.7. The particles are leaving from outlets, hence mass flow rate values are negative in the following Figure.

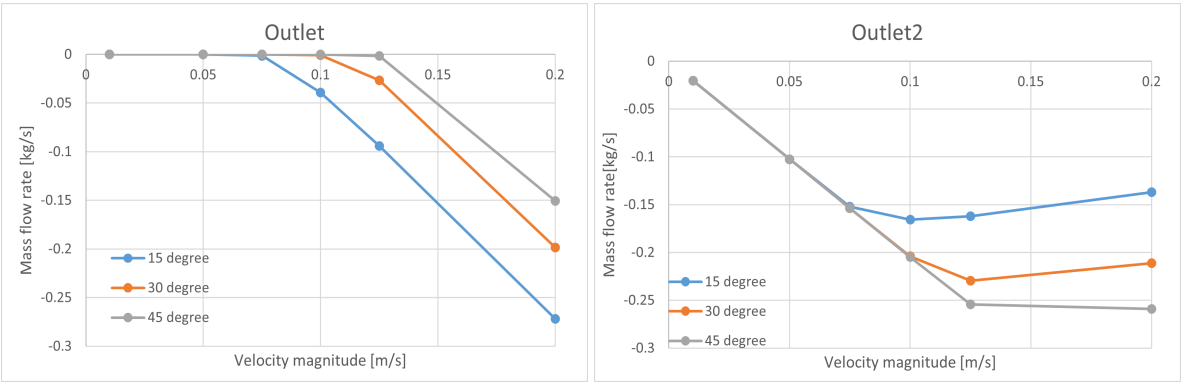

(a) Outlet

(b) Outlet2

Figure 4.22: Mass flow rate at outlet regarding the inclined angle

It can be observed from Figure 4.22 that when the inclination angle increases, the mass flow rate of leaving particle from outlet increases, and outlet 2 decreases. Also,

the total mass flow rate increases as the outlet increment are higher than outlet 2's reduction rate.

When the inclination angle increases, the fraction of particles leaving the top outlet decreases, which means that the sedimentation effectiveness increases. Hence, for greater inclination angles with the same velocity magnitudes, larger amount particles will sediment at the bottom of the system and it'll increase the effectiveness of the device. On the other side, if the angle would be much larger close to a 90-degree vertical column then the particles would not sediment at all as the terminal velocity is much smaller than the inlet velocity.

Chapter 5

Conclusion and Discussion

In conclusion, first set of analyses with basic vertical column geometries have been carried out. The comparison between Euler and DDPM model has been done to choose most fitting model for the GCI (time-step) analysis and consequent simulations. The results indicate that the Euler model can give the same results for larger time steps. Therefore, it saves much more computational time, and has less computational demand than DDPM model. In DDPM method, it's necessary to use smaller time steps. The sufficient time step is approximately 10 times smaller than the Euler method's 0.1s time step, otherwise, the incomplete particle tracking error occurs after a time.

For the time step analysis (GCI), it's hard to adapt that method to DDPM-KTGF model because of the non-continuous (particle) phase of the model, and that makes it hard to obtain balanced data from the slope of sedimentation analysis. Therefore, the Eulerian-Granular model is the better option for optimizing time steps rather than the DDPM-KTGF model for smaller particle analyses, which is highly time-consuming and computationally demanding.

Several analyses have been done with simplified geometries to find optimal time steps for specific sedimentation analysis. As a result of time step analysis, Euler model error rate (%) increases while the time step and total time are increasing. At the same time, the error ratio of the bigger time steps growth rate decreases, and the error ratio difference with the smaller time steps decreases. The optimal time step for the Euler model has been determined as 0.1 seconds.

Similarity analysis has been done to verify the possibility of using larger particle size instead of real particle size. Analysis with x μm sized particles is highly computational demanding and can take up to several days. Equation 3.32 had been used to compare the different sized particles sedimentation layers. The result of the first set of analyses

show that bigger particles can be used to reduce analysis time. Then, the Euler model and DDPM model had been compared against the real experimental data. As a result of the comparison, the Euler model is the better one and it has been decided to use for further analysis.

Furthermore, higher velocity shows effect on the sludge layer of the particles. The higher velocity magnitude expand the layer at the bottom of the lamella clarifier device and drags it to the top. The change of the values for each velocity magnitude for a specific angle can be seen in Figure 4.20. The particles are leaving from outlets, hence mass flow rate values are negative in the following Figure. When the velocity increases total mass flow rate and mass flow of leaving particle exponentially increasing. Also, the mass flow rate of leaving particles from the outlet increases, and from outlet 2 decreases. According to the results, the sedimentation effectiveness is better for greater inclination angles.

Figure 4.22 shows that when the inclination angle increases, the leaving mass flow rate of particles from outlet increases, and from outlet 2 decreases. The total mass flow rate increases as the outlet growth rate is higher than outlet 2's reduction rate.

When the inclination angle increases, the fraction of particles leaving the top outlet decreases, which means that the sedimentation effectiveness increases. Thus, for greater inclination angles with the same velocity magnitudes, larger amount particles will sediment at the bottom of the system and it'll increase the effectiveness of the device. On the other hand, when the angle becomes close to a 90-degree then the particles would not create a sediment layer at all as the terminal velocity is much smaller than the inlet velocity.

Table 5.1 expresses the effectiveness of leaving particles mass flow rate from the outlet. Where can be seen the effect of inclination angle and velocity magnitude clearly.

		velocity magnitude [m/s]					
		0.01	0.05	0.075	0.1	0.125	0.2
incl. angle	15°	100	99.99995	99.11805	80.78878	63.25276	33.52362
	30°	100	99.99999993	99.9969	99.59277	89.64826	51.54205
	45°	100	99.99999994	99.999995	99.97829	99.33119	63.2042

Table 5.1: Percentage (%) of Leaving Particles from Outlet 2

The critical velocity for 99 % effectiveness of lamella clarifier can be calculated by linear interpolation for each inclination angle. For the 15 degree, this velocity is between 0.075 [m/s] to 0.1 [m/s], for 30 degree, 0.1 [m/s] to 0.125 [m/s] and for 45 degrees, 0.125 [m/s] to 0.2 [m/s]. The results for 15 degrees is 0.075137 [m/s], for 30 degrees 0.10149 [m/s] and 45 degrees 0.125688 [m/s].

The present work is mainly aimed at reducing the computational demand and finding the optimal setup for the sedimentation analysis. Furthermore, to optimize the time step for the chosen model, GCI analyses had been used.

For further development, the number of analysis can be widened to find optimum inclination angle and velocity for the desired design of the lamella clarifier. Additionally, to fasten the sedimentation progress and get higher mass flow rates, a two-step lamella clarifier can be used. The first clarifier tank can have a higher velocity magnitude to reduce the number of particles faster during the first step and the second clarifier tank can have the optimal velocity to obtain higher effectiveness for the device.

Bibliography

[1]. Giuseppe B., Sustainable Management of Sediment Resources. Elsevier, 2007. vol. 2, pp. 1-10.

[2]. Portable Water Treatment, OpenLearn, viewed 25 December 2020. $< https : //www.open.edu/openlearn/science-maths-technology/engineering-and-technology/technology/potable-water-treatment/content-section-4.4 >$

[3]. Beyle, Andrey. Physical and Biochemical Risk Phenomena in Nanotechnology. Nanotechnology Safety, 2013, vol. 1, pp. 219–231.

[4]. Julien, Pierre Y. Erosion and Sedimentation, Cambridge University Press, 2010, vol. 2, no. 4, pp. 1-3.

[5]. Geankopolis, C. J.: Transport Processes and Separation Process Principles. New Jersey: Publishing as Prentice Hall PTR, 2003, vol. 4, pp .121-126.

[6]. Crowe, C. T. Multiphase Flow Handbook. CRC Press, 2016, vol. 2, pp. 17-21.

[7]. Doosan Škoda Power to supply steam turbine to Japan, 2020, Turbomachinary, viewed 25 December 2020, $< https : //www.turbomachinerymag.com/doosan-skoda-power-to-supply-steam-turbine-to-japan/ >$

[8]. Go-ahead for conversion first two Dutch wastewater treatment plants to revolutionary modular Verdygo concept, 2015, Dutch Water Sector, viewed 25 December 2020. $< https : //www.dutchwatersector.com/news/go-ahead-for-conversion-first-two-dutch-wastewater-treatment-plants-to-revolutionary-modular >$

[9]. Computational Fluid Dynamics: CFD Software, Simscale, viewed 25 December 2020, $< https : //www.simscale.com/product/cfd/ >$

[10]. “ANSYS Fluent Multiphase Tutorial- Multiphase Flow Modeling” ANSYS Customer Training Material, 2017

[11] S. Maulana, An Introduction to Computational Fluid Dynamics THE FINITE VOLUME METHOD, 2016, vol. 2, no. 2.

[12]. ANSYS Fluent User's Guide, ANSYS, Inc., 275 Technology Drive Canonsburg, PA 15317, 2020

[13] Roache, P., Perspective: A method for uniform reporting of grid refinement studies. ASCE Journal of Fluids Engineering, 1994, 116, 405-413 GCI page 24.

[14]. Examining Spatial (Grid) Convergence, 2008, NASA, viewed 25 December 2020, $< www.grc.nasa.gov/www/wind/valid/tutorial/spatconv.html >$

[15] Celik, I.B., Ghia, U., Roache, P.J., Freitas, C.J., Coleman, H and Raad, P.E. Procedure for estimation and reporting of uncertainty due to discretization in CFD applications, ASME Journal of Fluids Engineering,2008, v. 130 (7), pp. 078001-4.

[16]"Lamalla Clarifier." Wikipedia, Wikimedia Foundation, October 2013, viewed 15 June 2021 $< https://commons.wikimedia.org/wiki/File:Lamella_Clarifier_Schematic.png. >$

[17] McKean, T. Novel application of a lamella clarifier for improved primary treatment of domestic wastewater (PDF), 73rd Annual Water Industry Engineers and Operators' Conference, 2010, Bendigo Exhibition Centre: East Gippsland Water, Retrieved October 20, 2020.

[18] Development Document for the Final Effluent Limitations Guidelines and Standards for the Metal Products and Machinery Point Source Category (PDF) (Report). United States Environmental Protection Agency, 2003, Retrieved October 20, 2020.

[19] Water Environment Federation, Clarifier design (2nd edition), 2006, Maidenhead: McGraw-Hill Professional, ISBN 978-0071464161